Repeated Disuse Atrophy Imprints a Molecular Memory in Skeletal Muscle: Transcriptional Resilience in Young Adults and Susceptibility in Aged Muscle

Daniel C. Turner[1,2]*, Truls Raastad[1], Max Ullrich[1], Stian F. Christiansen[1], Hazel Sutherland[3], James Boot[4,5], Eva Wozniak[4], Charles Mein[4], Emilie Dalbram[6], Jonas T. Treebak[6], Daniel J. Owens[3], David C. Hughes[7], Sue C. Bodine[7], Jonathan C. Jarvis[3], Adam P. Sharples[1]*.

[1] Department for Physical Performance, Norwegian School of Sport Sciences, Oslo, Norway.
[2] Department of Molecular Medicine, University of Pavia, Italy.
[3] Research Institute for Sport and Exercise Sciences, Liverpool John Moores University (LJMU), Liverpool, United Kingdom.
[4] Genome Centre, Queen Mary University of London (QMUL), London, United Kingdom.
[5] Francis Crick Institute, London, United Kingdom.
[6] Novo Nordisk Foundation Center for Basic Metabolic Research, Faculty of Health and Medical Sciences, University of Copenhagen (UCPH), Copenhagen, Denmark.
[7] Aging and Metabolism Research Program, Oklahoma Medical Research Foundation (OMRF), Oklahoma City, Oklahoma, United States.

*Corresponding authors
Adam P. Sharples: adams@nih.no
Daniel C. Turner: daniel.turner@unipv.it

Abstract

Disuse-induced muscle atrophy is common after illness, injury, or falls, and becomes increasingly frequent with ageing. However, whether skeletal muscle retains a “memory” of disuse remains unknown. We investigated repeated lower-limb immobilization in young adults and a refined aged rat model of repeated disuse, integrating physiology, multi-omics, immunohistochemistry, biochemistry, and primary human cell analyses. In young human muscle, a second period of disuse elicited an attenuated transcriptional response in oxidative and mitochondrial pathways, suggesting a protective molecular memory, although this did not translate into attenuated atrophy. In contrast, aged muscle exhibited a detrimental molecular memory, with greater atrophy, exaggerated suppression of aerobic metabolism genes/pathways despite recovery of these genes after initial disuse, depletion of NAD^+ and mitochondrial DNA, and activation of proteasomal, extracellular matrix and DNA-damage pathways. Repeated disuse induced DNA hypermethylation and downregulation of aerobic metabolism and mitochondrial genes across species. *NR4A1* remained suppressed into recovery after initial disuse in young human muscle, whereas acetylcholine receptor subunit genes (e.g., *CHRNA1*, *CHRND*) were epigenetically primed in humans and further upregulated with repeated atrophy in both young and aged muscle. *NMRK2,* an NAD^+ biosynthesis gene, was among the most downregulated genes after both periods of atrophy in humans, and nicotinamide riboside (NR) improved myotube size in primary human muscle cells derived post-atrophy. These findings reveal that disuse atrophy imprints a molecular memory in skeletal muscle - attenuated transcriptional resilience in young adults yet exaggerated susceptibility in aged muscle.

Keywords: muscle memory, DNA methylation, aerobic metabolism, NAD^+ metabolism, *NR4A* family, AChR, *NMRK2*, nicotinamide riboside

Introduction

Age-related skeletal muscle loss (termed sarcopenia) is one of the main contributors to falling injury [1, 2, 3], often resulting in prolonged periods of disuse. Consequently, repeated falls in the elderly become increasingly common, leading to recurrent loss of skeletal muscle and thus increased risk of frailty, morbidity, hospital admittance, reduced quality of life and ultimately earlier mortality [2, 4, 5, 6, 7]. Restoration of skeletal muscle following periods of disuse is also impaired in aged muscle [5, 8, 9, 10, 11, 12], further increasing the risk of repeated falls [2, 3]. Despite the well-characterised skeletal muscle wasting (atrophy) response to a single period of limb immobilisation [8, 9, 10, 13, 14, 15, 16, 17, 18, 19, 20, 21], bed rest [22, 23, 24, 25, 26] and spaceflight [27, 28, 29], whether muscle atrophy is exacerbated upon repeated disuse in both adult and aged muscle is currently unknown.

Skeletal muscle "memory" refers to the differential tissue response to repeated exposure to the same (or similar) environmental stimuli [30, 31]. While it is evident that skeletal muscle exhibits a 'positive' memory of anabolic stimuli, resistance [32, 33, 34, 35, 36, 37, 38, 39] and endurance [34, 40] training in both humans and rodents, it is unknown whether skeletal muscle possesses a ´negative´ memory of disuse-induced muscle atrophy. Specifically, whether an earlier encounter of disuse renders the muscle more susceptible to further wasting if reencountered in the future following injury reoccurrence or repeated falling in the elderly.

Epigenetics is considered a key mechanism underpinning skeletal muscle memory, whereby retention of epigenetic modifications in skeletal muscle are either; a) modified following exercise training and retained during detraining, leading to sustained elevations in gene transcription [33, 34, 36, 37, 39, 40] and protein abundance [38] and/or; b) enhanced upon later retraining, resulting in amplified changes in gene expression [33, 34, 36, 37, 39, 40]. Among the various epigenetic modifications, DNA methylation is one of the most prominent emerging regulators of skeletal muscle memory. DNA methylation undergoes genome-wide alterations and modulates the transcriptional response to acute exercise and chronic training in divergent pathways according to the mode of exercise performed [33, 36, 37, 39, 40, 41, 42, 43, 44, 45, 46, 47, 48, 49, 50, 51, 52, 53, 54, 55]. Moreover, DNA methylation is dynamic and can both precede and modulate the time course of transient gene expression in skeletal muscle in the minutes to hours following a single bout of exercise (reviewed in [56]). However, some DNA methylation changes are long-lasting, particularly those induced by chronic training, thus providing a key mechanism mediating skeletal muscle memory of exercise [31, 33, 34, 36, 37, 39, 40].

Despite the epigenetic role in modulating gene transcription in response to positive stimuli, studies examining the DNA methylation response to negative stimuli such as muscle disuse atrophy remain scarce. Nevertheless, there is clear evidence of a dysregulated methylome in skeletal muscle of aged [57, 58, 59, 60, 61] and diseased populations (e.g., type-II diabetes [42, 51, 62] and cancer [48]), in which greater aerobic fitness (higher $\dot{V}O_{2max}$) [57], higher physical activity, or exercise training can recalibrate the nuclear [39, 48, 57, 58, 59] and mitochondrial methylome [63] toward epigenetic signatures resembling that of youthful

muscle. Following disuse atrophy, hypermethylation and reduced expression of targeted genes such as *PPARGC1A* after nine days of bed rest in human muscle [64], and *Nos1* after acute immobilization in mice [65] have been reported. Our group have also demonstrated hypomethylation and increased expression of E3 ligases (*Murf1* and *MAFbx/Fbxo32*), the acetylochline receptor subunit (*Chrna1*), and the histone deacetylase (*Hdac4*) following tetrodotoxin (TTX)-included disuse atrophy in young adult rat muscle [66]. To date, however, most studies have predominantly focussed on targeted gene methylation with limited data available on genome-wide methylation. A recent study combined methylome and transcriptome analyses after 2 weeks of disuse atrophy in young adult humans (via lower limb casting) and reported predominance of global hypermethylation that was associated with a larger number of downregulated versus upregulated genes [39]. However, leg casting-induced disuse was preceded by resistance training, and therefore it is unknown whether the such alterations occur following disuse atrophy without prior resistance training that is more representative of the general population [39]. A recent study analysing genome-wide DNA methylation in purified muscle stem cells (MuSC) following injury in adult mice demonstrated sustained differential methylation long after recovery [67], whereas myoblasts retain DNA methylation changes after repeated inflammatory exposure *in vitro* [68]. However, no studies have investigated the combined methylome and transcriptome following repeated atrophy to determine whether skeletal muscle imprints a ´negative´ memory of disuse-induced atrophy in both young adult and aged muscle.

Therefore, we sought to determine whether skeletal muscle exhibits a 'negative memory' of disuse atrophy. We hypothesized that prior episodes of disuse atrophy would induce persistent molecular imprints that exacerbate subsequent repeated atrophy, particularly in aged muscle. Due to frailty and therefore ethical issues associated with repeated atrophy in elderly humans; to test this, we combined comprehensive physiological, histological and molecular analyses in parallel young adult human and aged animal models of disuse atrophy, recovery and repeated atrophy. Here, we demonstrate that skeletal muscle retained a molecular memory of disuse. In young adults, repeated immobilization triggered a predominantly resilient and 'protective' transcriptional memory, characterised by attenuated transcriptional changes in aerobic metabolism and mitochondrial pathways following repeated disuse, despite full restoration of skeletal muscle after recovery. However, this did not lead to attenuated muscle loss after repeated atrophy. In contrast, aged muscle exhibited a detrimental susceptibility, characterised by an exaggerated suppression of aerobic metabolism and mitochondrial pathways, mtDNA loss, and muscle wasting despite recovery of these gene pathways after initial disuse. Proteasomal, extracellular matrix (ECM), and DNA-damage associated pathways were uniquely elevated in aged muscle to repeated disuse. Epigenomic profiling revealed conserved DNA hypermethylation in aerobic and mitochondrial gene networks across species to atrophy and repeated atrophy, alongside identification of locus-specific memory genes, *NR4A1* and AChR subunit genes. Finally, NAD^+ salvage with nicotinamide riboside (NR) improved myotube size in human primary MuSC derived post-atrophy.

Methods

Human ethics and participant information

Ethical approval was granted by the Regional Committees for Medical and Health Research Ethics (REK, Application ID 227924). The study was registered with the Norwegian Agency for Shared Services in Education and Research (Sikt) under reference number 627824. Participants were familiarised with the study intervention and the possible associated risks. Informed written consent and completion of an approved health and pre-biopsy medical questionnaire were obtained prior to participation. Ten young adults, males (*n* = 7) and females (*n* = 3) living in Oslo, Norway participated in the study. Participants were free from any known injury, illness and disease and had no previous history or predisposition to deep vein thrombosis (DVT). Participant baseline characteristics are presented in **Table 1**. All human data collection was conducted at the Norwegian School of Sport Sciences.

Table 1. Young adult human baseline characteristics. Values presented as mean ± standard deviation (SD).

	Male (*n* = 7)	**Female** (*n* = 3)	**All** (*n* = 10)
Age (yrs)	27.1 ± 4.1	23.7 ± 3	26.5 ± 4.1
Height (cm)	181.7 ± 2.7	167.9 ± 7.5	177.5 ± 7.9
Weight (kg)	93.4 ± 16	62 ± 12.6	84 ± 20.9
Body mass index, BMI (kg/m^2)	28.4 ± 5.3	21.8 ± 2.6	26.4 ± 5.5
Total Lean body mass, LBM (kg)	64.8 ± 4.4	41.5 ± 7.2	57.8 ± 12.3
Fat mass, FM (kg)	24.8 ± 13.1	18.3 ± 5.7	22.3 ± 11.4
Fat free mass, FFM (kg)	68.2 ± 4.5	43.9 ± 7.3	60.9 ± 12.8
Body fat, BF (%)	25.4 ± 9.4	29.1 ± 4.5	26.5 ± 8.2
Immobilised leg lean mass, LM (kg)	11.4 ± 1.2	7.4 ± 1.5	10.2 ± 2.3
Non-immobilised leg LM (kg)	11.5 ± 1.3	7.1 ± 1.6	8.9 ± 2.5

Assessment of physical activity levels and dietary intake in humans

The International Physical Activity Questionnaire Short Form (IPAQ-SF) was used to assess short-term physical activity levels prior to the study [68]. Participants also completed an additional non-validated questionnaire including questions related to the specific type of sport (e.g., team, endurance, speed/power) or activity (e.g. cardiorespiratory fitness, strength, concurrent), duration of participation and competition level (i.e. recreational, national, international) to assess long-term physical activity levels.

Human study design

In a repeated measures design, participants underwent 2 weeks (wks) (14 days/d) disuse atrophy (via unilateral limb immobilization) → ≈ 7 wks (49 ± 5 d) recovery → 2 wks repeated disuse atrophy (**Figure**

190 **1A**). During immobilisation, participants were fitted with a knee brace (DonJoy® X-Act ROM,
191 Enovis/DJO LLC, USA) fixed at 30° knee flexion to prevent any weight bearing of the non-dominant leg.
192 Crutches were provided to enable ambulation without weight bearing on the braced immobilised leg.
193 Following immobilisation, the knee brace and crutches were removed and participants returned to their
194 normal ambulatory activity for ≈ 7 wks to allow recovery. Finally, the same non-dominant leg underwent
195 a second period of 2 wks of immobilisation (repeated atrophy). Before immobilisation, participants were
196 trained using the crutches and knee brace and were instructed to only remove the knee brace for
197 showering and bedtime. Daily exercises (e.g., ankle rotation/dorsiflexion/plantarflexion) were
198 encouraged to reduce the risk of DVT[69] . There were no reported cases throughout the present study.
199 Before and after each immobilization, muscle biopsies and measurements of SkM size and strength
200 were conducted in the morning (± 1 hr between timepoints) under fasted conditions following the same
201 testing order (**Figure 1A**). Participants were also advised to refrain from strenuous exercise and alcohol
202 consumption 24 hrs prior to muscle biopsy and testing procedures. Muscle biopsies and the testing
203 protocol are detailed below. Upon completion of the study intervention, for ethical reasons, all
204 participants were provided with the opportunity to undertake supervised resistance training programme
205 (3 d/wk for 7 wks consisting of 2 lower body and 1 upper body sessions each wk) to restore any loss of
206 SkM. Two-four weeks of strength training is sufficient for restoring SkM following a similar duration of
207 atrophy in young adult humans [8, 11, 70].
208
209 *Human skeletal muscle biopsy procedures*
210
211 Muscle biopsies were obtained from the immobilised leg according to our procedures described
212 elsewhere [48, 49]. Briefly, local anaesthesia (Xylocaine with 10 mg/mL lidocaine + 5 µg/mL adrenaline,
213 AstraZeneca, Södertälje, Sweden) was administered to the biopsy area and muscle tissue (133 ± 47
214 mg excluding muscle tissue for immunohistochemical analysis, see below) was obtained from the mid-
215 belly (10% proximal of the mid-thigh) of the *m. vastus lateralis (VL)* muscle using a modified Bergström
216 technique (6 mm Pelomi-needle, Albertslund, Denmark) with manual suction (i.e., 50 mL syringe
217 connected to the Bergström needle). For immunohistochemical (IHC) analysis, a proportion (≈ 50 mg)
218 of muscle tissue was embedded in optimal cutting temperature (OCT) compound (CellPath, Chemi-
219 Teknik AS, Oslo, Norway) ensuring myofibres were aligned in parallel before freezing in pre-cooled
220 (i.e., above liquid nitrogen, LN_2) isopentane (Sigma-Aldrich, Oslo, Norway) placed on dry ice and stored
221 at −80 °C. Remaining tissue was rinsed in pre-cooled (4 °C) saline containing 0.9% NaCl (Braun,
222 Melsungen, Germany) and dissected to remove visible fat, connective tissue and blood (vessels).
223 Tissue intended for RNA, DNA and protein analysis was immediately weighed, transferred to nuclease-
224 free Eppendorf tubes (Invitrogen™ RNase-free Microfuge Tubes, Fisher Scientific, Oslo, Norway),
225 snap-frozen in LN_2 and stored at −80 °C. Remaining tissue used for *in vitro* experiments was submerged
226 in pre-cooled (4 °C) transfer media (Hams F-10 medium that includes 1 mM L-glutamine/LG, 0.2% heat
227 inactivated/hiFBS, 100 U/mL penicillin, 100 µg/mL streptomycin/PS and 2.5 µg/mL amphotericin-B/AB,
228 Fisher Scientific) for subsequent primary cell isolations detailed below.
229

Assessment of body composition in humans

Height (cm) and body weight (kg) were measured using a digital stadiometer and scale, respectively (Seca, Hamburg, Germany). Whole-body composition and leg lean mass (LLM) were assessed by dual-energy x-ray absorptiometry (DEXA; Lunar iDXA, enCORE software version 18; GE Healthcare, Chicago, USA). Total LLM was defined as all lean mass located distally from the collum femoris and inferior pubic ramus. A triangular segment depicting the pelvic area and a midline separating left and right legs were constructed as previously described [71]. Specifically, the horizontal line of the triangle segment transversed slightly above the two iliac crests, and the two angled lines crossed the collum femoris, meeting just below the genital area [71]. An additional line crossing the intercondylar eminence separated the upper and lower leg. All images were analysed single-blinded by three experienced personnel, and the average values were reported. The coefficient of variation (CV) for test-retest reliability was 1%.

Assessment of muscle cross-sectional area (mCSA) in humans

Muscle cross-sectional area (mCSA) of the *m. rectus femoris (RF)* and *VL* muscles were assessed using panoramic B-mode ultrasound scanning using a linear transducer (L18-5) fixed to an ultrasound system (MACH 30; Hologic SuperSonic Imagine™, Aix-en-Provence, France). During scanning, participants lay supine (knee angle at 0 °C) with their leg muscles relaxed and feet strapped to a stable box to prevent any hip rotation. Three measurements per muscle (*RF* and *VL* each scanned separately) were measured and analysed by following a transverse trajectory line drawn across the mid-thigh (i.e., 50% of the distance between the greater trochanter and distal end of the muscle) using a marker pen, demonstrating a low <2.5% CV across all timepoints (RF baseline 2.4 ± 1.1%, atrophy 1.6 ± 1%, recovery 2.1 ± 1.1%, repeated atrophy 1.8 ± 1.6%, VL baseline 1.7 ± 1.3%, atrophy 1.3 ± 0.7%, 1.8 ± 1% recovery, 1.6 ± 0.7% repeated atrophy). Only acquired images free from visible artefacts/stitching were considered acceptable for analysis. Participants were encouraged to redraw the trajectory line during the immobilization and recovery periods to ensure accurate probe repositioning during subsequent timepoints. A transparent plastic sheet was also used to mark the trajectory and other clear landmarks (e.g., scars, patella and other marks) to provide additional accuracy during rescanning. Finally, previous images were displayed during rescanning to confirm image acquisition accuracy between timepoints. All images were analysed single-blinded using ImageJ2 with Bio-Format plugin (version 2.14.0/1.54f, U. S. National Institutes of Health, Bethesda, Maryland, USA) [57,58] at the end of the intervention. One participant was excluded from all mCSA analyses due to inaccurate repositioning and/or visible imaging artefacts.

Assessment of muscle strength in humans

Voluntary maximal Isometric knee extension and flexion torque (Nm) was measured at 90, 60 and 30° knee flexion using a dynamometer (HUMAC NORM; Computer Sports Medicine inc, Massachusetts,

270 USA). Participants were first familiarised with the protocol one week prior to baseline testing. Prior to
271 strength testing, participants performed a standardised warm-up consisting of 5 mins low intensity
272 cycling, 5 mins stretching and 3 × submaximal efforts (50-80%). Following the warm-up, participants
273 performed 5 × maximal repetitions at each knee flexion angle (in order of 90, 60 and 30°). Verbal
274 encouragement was provided during each repetition. The greatest torque produced was considered
275 their maximum voluntary contraction (MVC). If the difference in torque between the first and second
276 strongest repetition was >5%, participants performed an additional repetition. MVC was acquired on
277 MP150 (Biopac, Goleta, CA, USA) with a sampling frequency of 1000 Hz and analysed using
278 AcqKnowledge software (version 4.4.2, Biopac Systems, Inc., Knivsta, Sweden).
279
280 *Animals and study design*
281
282 Ethical approval was obtained, and experimental procedures were conducted with the permissions
283 within a project license granted (PA693D221) under the British Home Office Animals (Scientific
284 Procedures) Act 1986. Aged (23 ± 1 months) male Fischer 344 rats (Charles River) weighing 354 ± 54
285 g were housed at 20°C and 45% relative humidity on an alternating 12 hr light and 12 hr dark cycle,
286 with food and water available *ad libitum*. Animals were assigned to 1 of 4 groups (*n* = 3 per group)
287 including a control group (sham control) and 3 experimental groups (atrophy, recovery and repeated
288 atrophy). All experimental groups received tetrodotoxin (TTX) to the common peroneal nerve (CPN),
289 preventing contraction of the ankle dorsiflexor muscles. TTX binds to the voltage-gated sodium channel
290 in the nerve cell membranes and so prevents the conduction of action potentials. Therefore, muscles
291 innervated by the blocked CPN cannot be activated to contract. This induces disuse atrophy of the hind
292 limb dorsiflexor muscles i.e., the tibialis anterior (TA) and extensor digitorum longus (EDL), and is
293 advantageous vs. denervation or hindlimb unloading as it allows normal conduction in the tibial nerve
294 to achieve plantarflexion, and therefore animals can undertake locomotion for daily living (**Figure 2A**)
295 [59–61]. The atrophy and recovery groups received a single infusion of TTX (6-7 d) followed by 9 d of TTX
296 abstinence (e.g., TTX → recovery), whereas the repeated atrophy group received a second TTX
297 infusion (5-6 d) following recovery (e.g., TTX → recovery → repeated TTX) (**Figure 2A**). The sham
298 control group consisted of *n* = 1 for each timepoint (TTX/recovery/repeated TTX) that received the same
299 surgical procedures (detailed below) as the experimental groups in the absence of TTX administration.
300 Pre- and post-intervention animal weights for each group are presented in **supplementary Table 1** and
301 muscle weights are provided in **Supplementary Figure 3.**
302
303 *Animal experimental procedures*
304
305 Surgical and TTX-administration procedures are described elsewhere [66, 72]. Briefly, animals were first
306 anaesthetized via inhalation of a gaseous mixture of 3% isoflurane in oxygen for induction and 1–2%
307 for maintenance prior to subcutaneous implantation of a mini osmotic pump (Mini Osmotic Pump 2002;
308 Alzet, Cupertino, CA) in the scapular region. Silicone tubing attached to the mini osmotic pump was
309 then passed under the skin to the site of the left common peroneal nerve (CPN). A second incision was

310 made laterally through the skin, just proximal to the knee joint and through the biceps femoris muscle
311 (posterior compartment of the thigh) to enable access to the CPN. A silicone cuff extending from the
312 silicone tubing was placed around the nerve. All incisions were closed in layers. The mini osmotic pump
313 (Mini Osmotic Pump 2002; Alzet, Cupertino, CA) delivered TTX to the CPN. The osmotic pump
314 successfully delivered 0.5 µl/hr TTX (350 mg/mL in sterile 0.9% saline), continuously blocking ankle
315 dorsiflexion for a 7d period after which the TTX was exhausted, while maintaining normal voluntary
316 plantarflexion via the tibial nerve. TTX was not administered to the right limb, and it served as a
317 contralateral control for each individual animal. For the repeated disuse atrophy experiments, the rats
318 were anaesthetized briefly after the recovery period. The empty osmotic pump was removed through
319 an interscapular incision and replaced with a new TTX-loaded pump. The welfare and mobility of the
320 rats were checked daily by animal welfare staff.
321
322 *Human muscle derived cell (MuSC) experimental procedures*
323
324 Isolation of human muscle derived cells (MuSC) and subsequent cell culture procedures are previously
325 described by our group [59, 72]. Briefly, pre- and post-atrophy muscle biopsies (*n* = 4 of pre- and post-
326 biopsies) were immediately transferred to a sterilised class II culture hood (Thermo Scientific MSC-
327 advantage) in low serum transfer media (components described above). Visible fat and connective
328 tissue were removed, and remaining muscle tissue was washed 3 × PBS (1× with added PS and AB),
329 before undergoing repeated rounds of scissor mincing in trypsin (0.5%)-EDTA (0.2%) and centrifugation
330 (340 × *g* for 5 min at 24 °C) to promote cell migration. The supernatant, cell pellet and remaining non-
331 homogenised tissue were seeded into separate T25 pre-gelatinised flasks containing 5 mL growth
332 media (GM: Ham's F-10, 10% hiFBS, 10% heat inactivated new born calf serum/hiNBCS, 2 mM LG,
333 PS and AB) and left unagitated in a humidified incubator (37 °C, 5%, VWR ILCO 180 Premium) for 5-7
334 d to promote cell growth. GM was changed every 2-3 d thereafter until sufficient cell attachment and
335 growth (<80% confluency within cell colonies) was achieved. MuSC were transferred and sub-cultured
336 in T75 flasks to further increase cell yield and ensure sufficient MuSC numbers for subsequent
337 experiments described below.
338
339 To determine the effects of disuse *in vivo* on differentiation capacity *in vitro*, both pre- and post-atrophy
340 MuSC (7×10^4 cells/mL in 2 mL of GM) were seeded onto pre-gelatinised six-well plates and left until
341 ≈ 80% confluency was attained (taking between 24 and 48 hrs). Cells were then washed 3 × PBS (1×)
342 and media was switched to low serum media (DM: same components as GM with lower 2% hiFBS) to
343 permit differentiation over 10 days (d). An additional 1 mL DM was added at 72 hrs and media was
344 switched to DM containing either 0.5 mM nicotinamide riboside (NR, ChromaDex Inc, USA), previously
345 used by out group [73] or control (H_2O) for both pre- and post-atrophy conditions. Cell pellets derived from
346 4 × wells at 0 hrs, 7 and 10 d (+/- NR supplementation) were snap-frozen and stored at -80 °C for later
347 copurification of DNA ($2 \pm 0.19_{A260/A280}/0.14 \pm 0.14_{A260/A230}$) and RNA ($2.05 \pm 0.03_{A260/A280}/1.86 \pm$
348 $0.48_{A260/A230}$) using the AllPrep RNA/DNA Mini Kit (Qiagen). The remaining 2 × wells were treated for
349 subsequent immunocytochemistry analysis described below. There was no difference in the proportion

350 of myoblasts (42 ± 22% versus 45 ± 26%, p = 0.62) and fibroblast (58 ± 22% versus 56 ± 26%, p =
351 0.62) in pre- and post-atrophy MuSC, respectively. Thus, MuSC were matched prior to differentiation
352 experiments. All MuSC were between passage 3 and 6 to avoid issues of cellular senescence [74].
353
354 *Immuno-histo/cytochemistry, imaging and analysis*
355
356 Serial sections at either 8 µm (human VL muscle) or 10 µm (mid-belly of the rat TA muscle) thickness
357 were made at −20 °C (CM1860, Leica Biosystems GmbH, Heidelberger, Germany), mounted on
358 microscope slides (Fisherbrand™ Superfrost™ Plus Microscope Slides, Fisher Scientific), air-dried for
359 30 mins and stored at −80 °C. When labelling muscle tissue samples, samples were first air-dried for
360 30 mins prior to blocking in 2% bovine serum albumin (BSA, Sigma-Aldrich) in 1× PBS (10 mM
361 phosphate buffer, 3 mM KCl, pH 7.4, Merck, Oslo, Norway) with 0.05% added tween (PBS-T, Tween®
362 20, VWR, Oslo, Norway) and 1% fat-free dry milk (Sigma-Aldrich) for 1 hr at room temperature (RT).
363 Muscle cross-sections were then counterstained for dystrophin (1:500; ab15277, Abcam, Cambridge,
364 UK), myosin heavy chain (MHC) type I (1:100; BA-F8, DSHB Supernatant, Schiaffino, S, Iowa, USA)
365 and MHC type IIA (1:100; SC-71, DSHB Supernatant, Schiaffino, S, Iowa, USA) diluted in 0.05% PBS-
366 T and 1% milk overnight at 4 °C (**Table 2**). After overnight incubation, samples were labelled with goat
367 anti-rabbit (GaR) IgG H+L (1:200; Alexa Fluor™ 488, cat. #A-11008 or Alexa Fluor™ 633, cat. #A-
368 21070**,** Thermo Fisher Scientific, Waltham, MA, USA), goat anti-mouse (GaM) IgG1 (1:200; Alexa
369 Fluor™ 488, cat. #A-21121) and/or GaM IgG2b (1:200; Alexa Fluor™ 594, cat. #A-21145) diluted in
370 0.05% PBS-T and 1% milk for 1 hr and RT (**Table 2**). Slides were washed 3 × 5 mins in 0.05% PBS-T
371 between each blocking and AB labelling steps. Finally, coverslips were mounted using ProLong™ Gold
372 Antifade Mountant with 4′,6-diamidino-2-phenylindole/DAPI (cat. #P36935, Thermo Fisher Scientific)
373 and left to air-dry at RT overnight prior to imaging. For imaging, tile scan images (1024×1024 frame
374 size) of whole cross-sections were acquired using a ZEISS LSM 800 (with Airyscan) confocal
375 microscope (ZEISS, Oberkochen, Germany) equipped with a 10×/0.3 objective and subsequently
376 processed using either ZEN 2 (blue edition, version 2.6) or ImageJ2 (version 2.14.0/1.54f, U. S. National
377 Institutes of Health, Bethesda, Maryland, USA) software. Automated analysis of myofibre cross-
378 sectional area (fCSA) and type was conducted using MyoVision 2.0 software [59]. Issues surrounding
379 muscle tissue processing in the human muscle (e.g., biopsy size, freeze damage) resulted in variable
380 sample numbers for average (type I and II combined; n = 8 for baseline/atrophy, n = 7 for recovery, n =
381 6 for repeated atrophy) and type I/II (n = 7 baseline, n = 8 atrophy, n = 6 recovery, n = 5 repeated
382 atrophy) myofibre analysis. The total number of fibres analysed from human biopsies was 398 ± 331
383 (average), 149 ± 94 (type I) and 281 ± 77 (type II). The total number of fibres analysed from whole rat
384 muscle was 6297 ± 2067 (average), 280 ± 109 (type I), 1237 ± 546 (type IIA), 69 ± 48 (type I/IIA), 4712
385 ± 1613 (type IIX/IIB).
386
387 For characterising myogenic (% myoblasts and fibroblasts) proportions and myotube differentiation,
388 MuSC were washed 3 × TBS (1×), fixed in 4% PFA for 15 mins, incubated in blocking/permeabilization
389 solution (5% goat serum/GS and 0.2% Triton X-100 in 1× TBS) for 1 hr at room temperature (RT). Cells

390 were then washed and incubated overnight (4 °C on a rocker) in Ab solution (2% GS and 0.2% Triton
391 X-100 in 1× TBS) containing anti-desmin (1:50; ab15200, Abcam) and TE-7 (1:100; CBL271, Merck)
392 primary Ab for counterstaining myoblasts and fibroblasts, respectively. After overnight incubation, cells
393 were washed 3 × TBS and incubated at RT for 3 hrs (4 °C on a rocker) in secondary Ab solution
394 containing anti-rabbit IgG TRITC (1:75; T6778, Sigma-Aldrich) for myoblasts and GaM Alexa Fluor®
395 488 (1:500; ab150117, Abcam) for fibroblasts. Finally, cells were washed 3 × TBS, prior to
396 counterstaining nuclei using DAPI (300 nM; D1306, Thermo Fisher Scientific) for 30 mins at RT. DAPI
397 was removed and stained cells were washed and stored in TBS for later image acquisition. The same
398 microscope and acquisition settings used for imaging tissue sections above were used when imaging
399 MuSC (2 × duplicate wells per condition/timepoint) except for acquiring nine (3 × 3) tile scan images.
400 The ImageJ2 cell counter was used to quantify the number of myoblasts and fibroblasts. The polygon
401 tool was used to outline the sarcolemma of all myotubes (cells with ≥3 nuclei) for assessing myotube
402 area (μm^2).
403
404 **Table 2.** Primary (1º) and secondary (2º) antibodies used for immunohistochemistry (IHC) and Western
405 blot (WB) procedures.
406

Application	Antibody	Supplier (cat. #)	Concentration	Species
IHC (1º)	anti-dystrophin	Abcam (ab15277)	1:500	Human/Rat
	BA-F8/anti-MHCI	DSHB	1:100	Human/Rat
	SC-71/anti-MHCIIA	DSHB	1:100	Rat
	Anti-Desmin	Abcam (ab15200)	1:50	Human
	TE-7 Anti-Fibroblasts	Merck (CBL271)	1:200	Human
	DAPI	Thermo Fisher (P36935)	in mountant	Human/Rat
	DAPI (*for MuSC*)	Thermo Fisher (D1306)	300 nM	Human
WB (1º)	OXPHOS	Abcam (ab110413)	1:500	Human/Rat
	CS	Abcam (ab96600)	1:4000	Human/Rat
IHC (2º)	GaR IgG (H+L) (Alexa Fluor 488)	Thermo Fisher (A-11008)	1:200	Human
	GaM IgG (H+L) (Alexa Fluor 488)	Abcam (ab150117)	1:500	Human
	GaR IgG (H+L) (Alexa Fluor 633)	Thermo Fisher (A-21070)	1:200	Rat
	GaM IgG1 (Alexa Fluor 488)	Thermo Fisher (A-21121)	1:200	Rat
	GaM IgG2b (Alexa Fluor 594)	Thermo Fisher (A-21145)	1:200	Human/Rat
	anti-rabbit TRITC	Sigma-Aldrich (T6778)	1:75	Human
WB (2º)	GaM IgG (H+L) HRP	Thermo Fisher (31430)	1:30000	Human/Rat
	GaR IgG (H+L) HRP	CST (7074)	1:3000	Human/Rat

407 DSHB = Developmental Studies Hybridoma Bank, CST = Cell Signalling Technology.
408

409 *RNA extraction from muscle tissue*

410

411 Skeletal muscle tissue derived from humans (33 ± 6 mg) and animals (27 ± 4 mg) was added to 2 mL
412 homogenizing mix tubes (Fisherbrand™, Fisher Scientific) containing 600 µl Buffer RLT (Qiagen) with
413 added 1% β-Mercaptoethanol (β-ME) before transferring to a tissue homogenizing instrument (MagNA
414 Lyser; Roche) for subsequent homogenization (3 × 45 s at 6000 rpm, placing samples on ice for 5 mins
415 between each disruption). Following homogenization, RNA was purified using a RNeasy® Mini kit
416 (Qiagen) and treated with DNase (RNAse-Free DNase Set, Qiagen) as per the manufacturer's
417 instructions. RNA quantity and purity for both human (128 ± 175 ng/mg tissue, 1.9 ± $0.1_{A260/A280}$/2.1 ±
418 $0.2_{A260/A230}$) and rat (406 ± 215 ng/mg tissue, 2.1 ± $0_{A260/A280}$/2.2 ± $0.2_{A260/A230}$) samples were quantified
419 via spectrophotometry (QIAxpert®, software version 2.4, Qiagen) and concentrations confirmed via
420 fluorometry (Qubit®, Qiagen). RNA integrity prior to sequencing was confirmed via Agilent Bioanalsyer
421 2100 with RIN scores 7.22 + 0.36 for human and 8.29 + 0.62 for rat samples (detailed below).

422

423 *qPCR for targeted mRNA analysis of aged rat muscle tissue and human MuSC*

424

425 Methods for mRNA expression analysis via qPCR by our group have been explained elsewhere [40, 48,
426 49, 59]. Briefly, a one-step QuantiFast SYBR Green kit (Qiagen) was used for preparation of PCR
427 reactions. Each 10 µl reaction contained 4.75 µl experimental sample (7.36 ng/µl totalling 35 ng per
428 reaction), 0.075 µl of both forward and reverse primer (100 µM stock) of the genes of interest (primer
429 details are provided in **Table 3**), 0.1 µl of reverse transcriptase and 5 µl of SYBR Green Master Mix
430 (totalling reactions). A thermocycler (Rotorgene 3000Q, Qiagen) was used to amplify target transcripts.
431 Reverse transcription was initiated with a hold at 50 °C for 10 mins (cDNA synthesis) and 5 mins at 95
432 °C (transcriptase inactivation and initial denaturation), before 40 cycles of; 95 °C for 10 s (denaturation)
433 followed by 60 °C for 30 s (annealing and extension). Only intended targets (via BLAST search) were
434 identified, thus yielding a single peak after melt curve analysis. All relative gene expression was
435 quantified using the comparative Ct ($^{\Delta\Delta}$Ct) method [75]. For *Nmrk2* expression analysis of aged animal
436 muscle tissue, C_T values (mean of technical duplicates) for each condition (atrophy/recovery/repeated
437 atrophy) were relativised to pooled C_T values from the control limb (*n* = 9) and reference gene, *Pol2ra*
438 (19.27 ± 0.41, 2.12% CV). For temporal mRNA analysis of *MRF* and *NMRK* genes in human MuSC, C_T
439 values (mean of technical duplicates) from pre- and post-atrophy MuSC at 7 and 10 d (+/- NR) were
440 relativised to own 0 hr C_T value and pooled reference gene, *RPL13A* (14.90 ± 0.43, 2.87% CV). To
441 determine the effects of NR supplementation, C_T values from 10 d +NR were relativised 10 d -NR and
442 pooled *RPL13A* values for both pre- and post-atrophy timepoints. Primers were designed using Basic
443 Local Alignment Search Tool (BLAST; http://blast.ncbi.nlm.nih.gov/) and Clustal Omega
444 (https://www.ebi.ac.uk/Tools/msa/clustalo/) and purchased from Sigma.

445

446

447

448

449 **Table 3:** qPCR primers

Species	Gene	Primer sequence (5' - 3')	Length (bp)	Reference
Human	***RPL13A***	F: GGCTAAACAGGTACTGCTGGG	105	Turner *et al.,* [59]
		R: AGGAAAGCCAGGTACTTCAACTT		
	MYOD	F: GCCACAACGGACGACTTCTA	117	Turner *et al.,* [59]
		R: GTGCTCTTCGGGTTTCAGGA		
	MYOG	F: TCCCAGATGAAACCATGCCC	103	Turner *et al.,* [59]
		R: AGGCCCCTGCTACAGAAGTA		
	NMRK1	F: AAATGTTGCTCCATACCATCCC	70	newly designed
		R: CTGCAGCTCCTAGTAATGCT		
	NMRK2	F: AGCTCTTCCGTGAAGTCCTG	62	newly designed
		R: TGATTCCTGGGAGCGGTTCA		
Rat	***Pol2ra***	F: GCTGGACCTACTGGCATGTT	102	Seaborne *et al.,* [72]
		R: ACCATAGGCTGGAGTTGCAC		
	Nmrk2	F: GCCGTATGAGGAATGCAAGC	90	newly designed
		R: ATGGGCCATACGTGACCATC		

450

451 *RNA-seq and associated bioinformatic analysis*

452

453 Total RNA (100 ng) from each sample was used to prepare mRNA libraries using the NEBNext mRNA
454 isolation kit in conjunction with the NEBNext Ultra II Directional RNA Library preparation kit (New
455 England Biolabs, Massachusetts, USA), and samples were randomised before preparation.
456 Fragmentation of isolated mRNA prior to first strand cDNA synthesis was carried out using incubation
457 conditions recommended by the manufacturer for an insert size of 300 bp (94 °C for 10 minutes). 13
458 cycles of PCR were performed for final library amplification. Resulting libraries were quantified using
459 the Qubit 4.0 spectrophotometer (Life Technologies, California, USA) and average fragment size
460 assessed using the Agilent 4200 Tapestation with D1000 screentape (Agilent Technologies,
461 Waldbronn, Germany). A final sequencing pool was created for each project using equimolar quantities
462 of each sample with compatible indexes. 59 bp paired-end reads were generated for each library using
463 the Illumina NextSeq 2000 in conjunction with the NextSeq 2000 P3 100 cycle kit (Illumina Inc.,
464 Cambridge, UK). Resulting FastQ files were imported and processed in Partek Flow® software (version
465 12.4.0; Partek, Inc. Missouri, USA) to filter contaminants (rDNA/tRNA/mtrDNA) using Bowtie 2 (version
466 2.2.5) and align reads to the hg38 *Homo sapiens* (release 39) and rn7 *Rattus norvegicus* genome
467 assemblies using Spliced Transcripts Alignment to a Reference (STAR) alignment tool (version 2.7.3a)
468 [76]. Total number of pre/post-aligned reads was 35/34 million and 49/49 million for human (65 bp average
469 read length) and rat (59 bp average read length) samples, respectively. Phred scores were >33 for both
470 human and rat RNA samples, thus trimming and filtering of reads was not required. Normalised
471 differential gene expression analysis was performed using *DESeq2* median of ratios [77]. Principal
472 component analysis (PCA), cluster heatmaps and volcano plots were created in R studio [78]. Venn
473 diagrams were redrawn from the open-source DeepVen web application[79]. Pathway (KEGG and
474 REACTOME) and gene ontology (GO; cellular component/CC, molecular function/MF and biological

475 process/BP) performed via the Database for Annotation, Visualization, and Integrated Discovery
476 (DAVID) knowledgebase [80] and associated figures created in R studio. Custom background gene lists
477 of detected genes following *DESeq2* normalization were used for functional annotation analysis. For
478 human analysis, normalised reads for each timepoint (atrophy/recovery/repeated atrophy) were
479 relativised to baseline. For rat samples, all experimental conditions in the left limb
480 (atrophy/recovery/repeated atrophy) were relativised to pooled right contralateral non-surgical limb.
481 Given there were no DEGs detected between sham and pooled contralateral control limb samples, we
482 excluded sham samples from further analysis and pooled contralateral non-surgical limb samples for
483 the control group. Genes with a ≥20% fold change (FC) and false discovery rate (FDR) of ≤5% are
484 considered differentially expressed genes (DEGs). Data are presented as either $\log_2$ or FC ± confidence
485 intervals (CI). Genes with negative changes presented as signed FC (-1/ratio). To perform temporal
486 clustering of the identified DEGs and DMRs (described below), self-organising map (SOM) profiling was
487 conducted using Partek Genomics suite, as previously described [38, 40, 46, 59]. SOM analysis plots a
488 standardised mean (z-score normalisation) shifting the mean to a value of 0 and scaling to a standard
489 deviation of 1. Therefore, by subtracting the mean of the group this centres the data around zero and
490 then dividing by the standard deviation, scales the data so the spread is consistent, allowing removal
491 of the absolute differences and focusing on relative changes allowing comparison of gene transcripts
492 and DMRs on a common scale. The mapping then clusters DEGs and DMRs based on similar temporal
493 profiles allowing visualisation of temporal signatures over time relative to the group mean. Also, this
494 allows the temporal signature of the DEGs and DMRs on common genes to be compared on the same
495 scale over the time-course of the intervention.
496
497 *DNA extraction from muscle tissue*
498
499 Skeletal muscle tissue derived from humans (21 ± 3 mg) and animals (12 ± 2 mg) was added to 2 mL
500 homogenizing mix tubes (Fisherbrand™, Fisher Scientific) containing 180 µl Buffer ATL (Qiagen,
501 Hilden, Germany) before transferring to a tissue homogenizing instrument (MagNA Lyser; Roche,
502 Basel, Switzerland) for subsequent homogenization (3 × 45 s at 6000 rpm, placing samples on ice for
503 5 mins between each disruption). Following homogenization, 20 µl proteinase K (Qiagen) was added
504 and samples were incubated at 56°C until complete lysis (≈ 30-60 mins) before continuing with DNA
505 purification using a DNeasy® Blood & Tissue kit (Qiagen) as per the manufacturer's instructions. DNA
506 quantity and quality for both human (251 ± 47 ng/mg tissue, 2 ± $0_{A260/A280}$/2.1 ± $0.1_{A260/A230}$) and rat (1427
507 ± 426 ng/mg tissue, 2 ± $0_{A260/A280}$/2 ± $0.1_{A260/A230}$) samples were quantified using spectrophotometry
508 (NanoDrop™ 2000; Thermo Fisher Scientific) and concentrations confirmed via fluorometry (Qubit®,
509 Qiagen). DNA integrity was confirmed prior to sequencing via Agilent Bioanalsyer 2100 with DIN scores
510 7.11 ± 0.17 for human and 7.22 ± 0.23 for rat samples.
511
512
513
514

515 *Reduced Representation Bisulfite Sequencing (RRBS): Library preparation and sequencing*
516
517 RRBS libraries were prepared from 100 ng of genomic DNA using the Diagenode Premium RRBS v2
518 library preparation kit, as per the manufacturer's protocol. For human samples, two pools of 8 samples,
519 and three pools of 7 samples were prepared after qPCR quantification of adapter-ligated sample and
520 prior to bisulphite conversion. 14 cycles of final library amplification were performed after assessment
521 of bisulphite converted library pool by qPCR. For rat samples RREM (reduced-representation enzymatic
522 methyl-seq) libraries were prepared using 100 ng of genomic DNA in conjunction with the NEBNext
523 Enzymatic Methyl-Seq kit (New England Biolabs, Massachusetts, USA). Briefly, DNA samples were
524 digested using MspI restriction enzyme followed by end-repair and adapter ligation. A two-step
525 enzymatic conversion was then performed by Oxidation of 5mC and 5hmC using TET2 and
526 glucosylation of 5hmC using T4-BGT. Deamination of unmodified cytosines was subsequently
527 performed using APOBEC. Converted samples were then uniquely barcoded and amplified by PCR
528 prior to sequencing. Libraries were sequenced using the Illumina NextSeq 2000 with P3 SBS 100-cycle
529 sequencing kit for human, and with P4 XLEAP 100-cycle sequencing kit for rat, both generating 50 bp
530 paired-end reads.
531
532 *RRBS quality control, trimming, alignment and methylation calling*
533
534 Reduced representation bisulfite sequencing (RRBS) libraries were processed using a standard
535 workflow. Raw base-call files were demultiplexed using Illumina `bcl2fastq /2.19.1`, and unique
536 molecular identifiers (UMIs) were extracted using `umi_tools` [81]. Reads were adapter and quality-
537 trimmed (minimum phred score 30) with `trim_galore` (https://doi.org/10.5281/zenodo.5127898). in
538 RRBS mode, reads less than 15 bp after trimming were discarded. Trimmed reads were aligned to the
539 human reference genome (hg38) or rat genome Rn6 using `bismark/0.22.1` [82] with `bowtie2`, with
540 the PBAT option enabled. PCR duplicates were removed with `deduplicate_bismark` in a UMI-aware
541 manner. CpG methylation calls were obtained using `bismark_methylation_extractor`.
542
543 *RRBS: Identification of differentially methylated positions (DMPs) and regions (DMRs)*
544
545 Downstream analysis was performed in R. Per-CpG coverage files were imported into `methylKit` [83]
546 with sites of low (<10 reads) or extreme coverage (top 0.1%) removed and outlier samples excluded.
547 For humans, data from each sample was then merged based on only CpGs present in at least 6
548 samples. Each of our groups contained 7-8 samples after outlier removal, making this threshold a
549 minimum of 75% of samples and giving a total of ≈ 1.8 million total CpGs analysed. For rats, there were
550 9 samples (3 per experimental condition of atrophy, recovery and repeated atrophy) and 9 samples for
551 the contralateral control limbs, therefore data from each sample was merged based on CpGs present
552 in all samples (100%), giving a total of 29K CpGs analysed. Differential methylation was identified at
553 individual CpGs (DMPs) and then 1-kb tiled regions (DMRs) using `calculateDiffMeth`. The

554 percentage methylation of each CpG was calculated using the percMethylation function in methylKit
555 and during differential analysis the mean percentage methylation of each CpG was calculated for each
556 group. For DMRs, mean percentage methylation for each experimental group was calculated by
557 averaging the percentage methylation of all CpGs within a given DMR across all samples from the given
558 group. For humans, we performed 6 pairwise comparisons of: 1) Atrophy vs. Baseline, 2) Recovery vs.
559 Baseline, 3) Repeated Atrophy vs. Baseline, 4) Recovery vs. Atrophy, 5) Repeated Atrophy vs.
560 Recovery, 6) Repeated Atrophy vs. atrophy. For rat analysis we performed: 1) Atrophy vs. Control, 2)
561 Recovery vs. Control, 3) Repeated atrophy vs. Control, 4) Recovery vs. Atrophy, 5) Repeated Atrophy
562 vs. Recovery, 6) Repeated atrophy vs. atrophy. For the rats, as with the transcriptome data, control was
563 determined as the pooled right/non-surgical limb (contralateral control limb = 9). Differentially
564 methylated CpGs and regions were annotated to genes and regulatory features for humans using
565 TxDb.Hsapiens.UCSC.hg38.knownGene(https://doi.org/10.18129/B9.bioc.TxDb.Hsapiens.UCSC.hg3
566 8.knownGene), org.Hs.eg.db (https://doi.org/10.18129/B9.bioc.org.Hs.eg.db) and annotatr
567 (https://doi.org/10.18129/B9.bioc.annotatr) and in rats using TxDb.Rnorvegicus.UCSC.rn6.refGene
568 (https://doi.org/doi:10.18129/B9.bioc.TxDb.Rnorvegicus.UCSC.rn6.refGene) and rg.Rn.eg.db
569 (https://doi.org/doi:10.18129/B9.bioc.org.Rn.eg.db). Default settings were used unless otherwise
570 specified. Only DMRs with FDR ≤ 0.05 were considered significant. SOM clustering (described above)
571 was performed on significant DMRs using percentage difference methylation as this allowed
572 methylation values at baseline (human) and control (rat) to enable temporal profiling.

573

574 *Mitochondrial DNA content*

575 Mitochondrial DNA (mtDNA) content was assessed via real time quantitative polymerase chain reaction
576 (RT-qPCR). PCR primers encoding for nuclear DNA (nDNA) markers; β_2 microglobulin (*B2M*),
577 hemoglobin subunit beta *(HBB)*, tubulin-specific chaperone A (*Tbca*), glyceraldehyde 3-phosphate
578 dehydrogenase (*Gapdh*), and mtDNA markers; mitochondrial 16S rRNA (*MT-RNR2*), D-loop region
579 (*DLOOP*), cytochrome B (*CYTB*), mitochondrially encoded 16S rRNA (*mt-Rnr2*) and 12S ribosomal
580 RNA (*mt-Rnr1),* were used to determine nuclear and mitochondrial DNA copy number, respectively.
581 Primer information is presented in **Table 4.** For qPCR, 20 ng DNA (9.6 µl at 2.08 ng/µl in nuclease-free
582 H_2O) was added to 10 µl SYBR® Green Mastermix (Qiagen) and 0.2 µl primers (100 µM stock, 1 µM
583 final concentration) to ensure 20 µl reaction volume. DNA was then amplified using a Rotor-Gene Q 5-
584 Plex HRM thermocycler (Qiagen) with supporting software (version 2.3.1). Thermal cycle settings
585 consisted of 3 mins at 95 °C (initial denaturation), followed by 40 cycles of 10 s at 95 °C, 30 s at 62 °C
586 (annealing) and final extension of 10 s at 95 °C. Melt curve analysis was performed at 0.5 °C increments
587 from 65 to 95 °C. Mitochondrial DNA content was reported as the ratio of mtDNA (*16S, CYTB* and/or
588 *DLOOP* for human; *mt-Rnr2* and/or *mt-Rnr1* for rat) to pooled nDNA (*B2M/HBB* for human; *Tbca/Gapdh*
589 for rat) determined using the $^{\Delta\Delta}$Ct method [75, 84].
590
591

592 **Table 4.** Primers used for encoding for nuclear DNA (nDNA) and mitochondrial DNA (mtDNA) markers
593 for assessment of mtDNA content.
594

Species	Gene	Primer sequence (5' - 3')	Length (bp)	Reference
Human	***B2M***	F: TGCTGTCTCCATGTTTGATGTATCT	86	Lapatto *et al.,* [85]
	(nDNA)	R: TCTCTGCTCCCCACCTCTAAGT		
	HBB	F: CAGGTACGGCTGTCATCAGTTAG	185	Lapatto *et al.,* [85]
	(nDNA)	R: CATGGTGTCTGTTTGAGGTTGCT		
	DLOOP	F: CATCTGGTTCCTACTTCAGGG	106	Lapatto *et al.,* [85]
	(mtDNA)	R: CCGTGAGTGGTTAATAGGGTG		
	CYTB	F: GCCTGCCTGATCCTCCAAAT	132	Lapatto *et al.,* [85]
	(mtDNA)	R: AAGGTAGCGGATGATTCAGCC		
	MT-RNR2	F: GGGGCGACCTCGGAGCAGAA	213	Lapatto *et al.,* [85]
	(mtDNA)	R: ATAGCGGCTGCACCATCGGGA		
Rat	***Tbca***	F: TGTCCCACCTGTTTGTTCTCT	50	Kemper *et al.,* [86]
	(nDNA)	R: GGTCCTTGGACACCTAGACG		Arduini *et al.,* [87]
	Gapdh	F: GGAAAGACAGGTGTTTTGCA	129	Stevanovic-Silva *et al.,* [88]
	(nDNA)	R: AGGTCAGAGTGAGCAGGACA		
	mt-Rnr1	F: CTCAAGACGCCTTGCCTAGC	131	Kemper *et al.,* [86]
	(mtDNA)	R: TCGTATGACCGCGGTGGCT		Arduini *et al.,* [87]
	mt-Rnr2	F: AGCTATTAATGGTTCGTTTGT	132	Stevanovic-Silva *et al.,* [88]
	(mtDNA)	R: AGGAGGCTCCATTTCTCTTGT		

595
596 *Protein extraction and Western blot*
597
598 Skeletal muscle tissue derived from humans (21 ± 6 mg) and rats (38 ± 14 mg) was added to 2 mL
599 homogenizing mix tubes (Fisherbrand™, Fisher Scientific) containing either 1 mL RIPA buffer (Thermo
600 Fisher Scientific) with added protease and phosphatase inhibitors (Halt™ inhibitor cocktail, Thermo
601 Fisher Scientific) for human samples or sucrose lysis buffer (250 mM sucrose, 50 mM Tris pH 7.5, 1
602 mM EDTA, 1 mM EGTA, 1% Triton™ X-100, Sigma-Aldrich) with added inhibitors (Thermo Scientific™
603 Pierce Mini Tablets, Thermo Fisher Scientific) for rat samples. Tubes were then transferred to a MagNA
604 Lyser instrument (Roche) for subsequent homogenization (3 × 45 s at 6000 rpm, placing samples on
605 ice for 5 mins between each disruption). Following homogenization, protein concentration was
606 quantified for both human (73 ± 13 µg/mg) and rat (84 ± 18 µg/mg) tissue via the bicinchoninic acid
607 (BCA) method (Pierce™ BCA protein assay kit, Thermo Fisher Scientific) and a FLUOstar Omega
608 microplate reader (BMG LABTECH, Ortenberg, Germany) with supporting software (Omega version
609 1.3). For Western blotting, protein aliquots were first diluted in 4× Laemmli Sample Buffer (Bio-Rad)
610 with added 0.5 M Dithiothreitol (DTT, Bio-Rad) and heated at either 45°C (oxidative phosphorylation,
611 OXPHOS) or 70°C (citrate synthase, CS) for 10 mins. Following denaturation, 20 or 25 µg for all protein
612 samples (in 15 µL for human and 20 µL for rat) and 5 µL protein marker (10-250 kDa, Precision Plus
613 Protein™ All Blue Prestained Protein Standards, Bio-Rad) were loaded into pre-cast gels (12 or 15 well,

614 4–20% Mini-PROTEAN® TGX Stain-Free™, Bio-Rad) before undergoing protein separation via
615 electrophoresis (200 volts/V for 30 mins). The current was monitored (A) pre- and post-electrophoresis.
616 Following electrophoresis, gels were activated under UV light ChemiDoc MP Imaging System (Bio-Rad)
617 and proteins transferred to PVDF nitrocellulose membranes (0.2 µm, Bio-Rad) using transfer stacks
618 (Bio-Rad) and a Trans-Blot Turbo Transfer System (Bio-Rad). Following protein transfer, membranes
619 were blocked (5% milk in 1% PBS-T for 1 hr at RT) and subsequently labelled with primary antibodies
620 against mitochondrial OXPHOS complexes (CI-NDUFB8, CII-SDHB, CIII-UQCRC2, CIV-MTCO1, CV-
621 ATP5A) (1:500, cat. #ab110413, Abcam) and CS (1:4000, cat. #ab96600, Abcam). Primary Ab were
622 diluted in 1% milk in 1% PBS-T and incubated on a roller overnight at 4 °C. After overnight incubation,
623 OXPHOS and CS proteins were labelled with secondary antibodies, GaM IgG (H+L) HRP (1:30000,
624 cat. #31430, Thermo Fisher Scientific) and GaR IgG (H+L) HRP (1:3000, cat. #7074, Cell Signaling
625 Technology), respectively. Membranes were washed (3 × 5 mins in 1% PBS-T) between blocking and
626 antibody labelling steps. Finally, membranes were incubated in enhanced chemiluminescence (ECL)
627 HRP substrate (SuperSignal™ West Dura Extended Duration Substrate, Thermo Scientific) for 5 mins
628 at RT to enable visualisation of membrane-bound proteins via chemiluminescence using a ChemiDoc
629 MP system (Bio-Rad) and analysis of band intensities using supporting software (Image Lab 6.1, Bio-
630 Rad). For human samples, all timepoints for each participant were loaded on the same gel and repeated
631 to ensure duplicate samples across two separate gels. Band intensities were relativised to own baseline
632 sample for subsequent timepoints (atrophy/recovery/repeated atrophy) and the average across the 2
633 gels was reported. One human recovery sample was excluded from all analysis due to low detection of
634 protein. Thus, there was n = 8 (rather than n = 9) samples for recovery timepoint. Similarly for aged
635 animal samples, the left/surgical and right/non-surgical limbs for each animal and condition (excluding
636 repeated atrophy as the protein lysates were low quality and quantity) were loaded on the same gel
637 across two separate gels. Band intensities of left/surgical limb were relativised to thier own right/non-
638 surgical limb for each condition (sham/atrophy/recovery). Control samples consisting of a mixture of all
639 human or rat samples were loaded in duplicate within each gel to ensure consistent sample loading.
640 There was no CII-SDHB band detected in 1 out of the 2 gels for both human and rat samples. Therefore,
641 data is derived from only one gel for this protein.
642
643 *NAD^+ measurements*
644
645 NAD^+ levels were measured using an enzymatic cycling assay [89]. Briefly, 11 ± 1 mg (human) and 8 ± 2
646 mg (rat) muscle were lysed in 400 µl 0.6 M perchloric acid ($HClO_4$) and homogenized using steel beads
647 and a TissueLyser II (Qiagen). Following homogenisation, samples were centrifuged for 5 min at 13,000
648 *g.* The supernatant was transferred to new tubes and neutralized in 100 mM Na_2HPO_4 (1:300 for human,
649 1:800 for rat). For the assay, 100 µl of diluted extract was pipetted into a white 96-well plate after which
650 100 µl of reaction mix was added. The reaction mix contained: 100 mM Na_2HPO_4, 10 µM
651 flavinmononucleotide, 2 % ethanol, 90 U/mL alcohol dehydrogenase, 130 mU/mL diaphorase, 2.5
652 µg/mL resazurin, and 10 mM nicotinamide. A Hidex Sense Microplate Reader (Hidex, Finland) was
653 used to measure the fluorescence of accumulated resorfurin (Ex 544 nm/ Em 580 nm) for 30 min

654 immediately after the reaction mix was added. Samples were run in duplicates and NAD^+ content was
655 calculated from the increase in fluorescence of a dilution series of NAD^+. Values were normalized to
656 protein concentration by dissolving the resultant pellets from the previous centrifugation step in 0.2 M
657 NaOH via heating to 95°C. Protein concentrations were determined using the bicinchoninic acid (BCA)
658 assay (Pierce™ BCA protein assay kit, Thermo Fisher Scientific).
659
660 *Statistical Analysis*
661
662 A Shapiro-Wilk´s test of normality was first performed for all physiological (e.g., body weight, SkM mass,
663 strength, mCSA and fCSA), protein abundance, mtDNA content and NAD^+ measurements. A repeated
664 (for human) or between (for aged animals) measures one-way analysis of variance (ANOVA) with
665 Tukey´s HSD post hoc detected significant ($p \leq 0.05$) differences whenever data was normally
666 distributed. Whenever data was non-normally distributed, a Friedman (for human) or Krustal-Wallis (for
667 aged animals) test with follow-up Dunn´s post hoc was carried out. For human myofibre (fCSA and fibre
668 type) analysis, a mixed-effect model was performed due to differences in sample number across
669 timepoints. For animal body weight (individual conditions), myofibre, mtDNA and NAD^+ content
670 analyses, a two-way ANOVA (within subject factor: limb, between subject factor: condition/timepoint)
671 with Tukey´s HSD post hoc was performed. For mean animal body weight across all conditions, an
672 unpaired t-test was performed. All statistical analysis was conducted in GraphPad Prism software for
673 macOS (version 10.4.1, Massachusetts, USA) and associated figures were created using GraphPad or
674 R studio for macOS (version 4.4.3). All data are presented as mean ± standard deviation (SD) unless
675 otherwise stated in the figure legends. RNA-seq and RRBS data statistical analyses are described
676 above.
677
678 **Results**
679
680 *Atrophy and repeated atrophy results in loss of leg lean mass, skeletal muscle size and strength in*
681 *young adult humans, with full recovery after initial disuse*
682
683 In young adult humans, the first period of disuse-induced atrophy (hereafter referred to as "atrophy")
684 resulted in a significant -3.6% reduction in total leg lean mass of the immobilised limb ($p = 0.005$, **Figure**
685 **1B**). Upon returning to normal habitual activity (i.e., "recovery"), mass was fully restored to pre-atrophy
686 baseline levels (p = *N.S* recovery vs. baseline). The second period of disuse (i.e., "repeated atrophy")
687 led to a similar significant -3.2% loss compared to previous recovery ($p = 0.004$, **Figure 1B**). Further
688 assessment of *vastus lateralis (VL)* and *rectus femoris (RF)* anatomical muscle cross-sectional area
689 (mCSA) in the immobilised limb revealed a -9% reduction in *VL* mCSA after initial atrophy ($p = 0.0003$),
690 that was fully restored during recovery (recovery vs. baseline, p = *N.S,* **Figure 1C***). Vastus lateralis*
691 mCSA was also significantly reduced after repeated atrophy relative to both baseline (-10.6%, p =
692 0.0003) and previous recovery (-8.9%, $p = 0.002$, **Figure 1C**). *Rectus Femoris* mCSA was only
693 significantly reduced after repeated atrophy relative to recovery (-3.5%, $p = 0.02$, **Figure 1D**). There

694 were no significant changes in the non-immobilised limb for total lean leg mass (**Supplementary Figure**
695 **1A-F)** or *VL* and *RF* mCSA (*p* = *N.S*, **Supplementary Figure 1 G-J**). There was however a significant
696 increase in lower leg lean mass of the non-immobilised limb during both periods of disuse periods
697 possibly due to a greater reliance on plantarflexor and dorsflexor muscles to support balance and
698 locomotion during immobilization of the opposite limb (**Supplementary Figure 1F**).
699
700 Concomitant with the loss of leg lean mass and quadriceps muscle size was a significant reduction in
701 knee extension strength (assessed via MVC) at 90° (-14.3%, *p* = 0.02) and 60° (-12.5%, *p* = 0.02) knee
702 flexion following initial atrophy that was also fully restored during recovery (*p* = *N.S*) **(Figure 1E & F)**.
703 Repeated atrophy induced a similar loss of strength at 90° (-13.8%, *p* = 0.02) and 60° (-14.3%, *p* =
704 0.002) following recovery (**Figure 1E & F**). Despite this loss of muscle strength at 60° and 90°, there
705 were no significant changes in knee extension MVC at 30° knee flexion (*p* = *N.S*, **Figure 1G**).
706 Concurrent reductions in size and strength also resulted in impaired muscle quality (e.g., specific force
707 by normalizing MVC to mCSA) (**Supplementary Figure 2A-I**). Specifically, MVC at 90° knee flexion
708 when normalised to *RF* mCSA was significantly reduced after atrophy (-12.8%, *p* = 0.05,
709 **Supplementary Figure 2D),** where repeated atrophy led to the greatest loss of specific force at 60°
710 when normalised to *VL* (-7.1%, *p* = 0.03), *RF* (-12.2%, *p* = 0.04) and *VL*+*RF* mCSA combined (-8.2%,
711 *p* = 0.02, **Supplementary Figure 2B & E & H** respectively). Finally, repeated atrophy led to significantly
712 reduced knee flexion torque at 90° (*p* = 0.03*,* **Supplementary Figure 2J**). Mean MVC at 60° and 30°
713 knee flexion also demonstrated the same trend but did not reach statistical significance (*p* = *N.S,*
714 **Supplementary Figure 2 K & L**)

715 At the myofibre level, IHC analysis revealed an average reduction in fibre type-specific cross-sectional
716 area (fCSA) after atrophy which approached significance when pooling fast and slow fibres (**Figure 1H-**
717 **K**). However, due to limited fibre number in the cross-sections from fewer samples in specific conditions,
718 we also used the open-source "FibeRtypeR" [90] web application to predict fibre type proportions using
719 RNA-seq gene lists, with this analysis suggesting a significantly greater proportion of type II fibres at
720 baseline (60% type II vs. 40% type I, *p* = 0.01), atrophy (67% type II vs. 33% type I, *p* < 0.001) and
721 repeated atrophy (63% type II vs. 37% type I, *p* = 0.003) with no significant difference after recovery
722 (61% type II vs. 39% type I, *p* = 0.05) (**Figure 1L**). Overall, demonstrating a reduction in the number
723 type I fibres and an increase in type-II fibres with both atrophy and repeated atrophy and a return to
724 baseline proportions with recovery (**Figure 1L**). From these gene lists, we next interrogated all essential
725 and regulatory fast (*MYL1, MYLPF*), slow (*MYL2, MYL3, MYL6B*) and fetal myosin light chains (*MYL6*)
726 as well as adult (*MYH7, MYH2, MYH1*) and developmental (*MYH3*, *MYH8*) myosin heavy chains
727 (**Figure 1M & N)**. On average, all 6 myosin light chains decreased after atrophy, were fully restored
728 after recovery and then reduced again after repeated atrophy. The slow *MYL2* and *MYL6B* genes were
729 significantly downregulated after atrophy (**Figure 1M)**. A similar temporal profile was observed for
730 slow(er) adult *MYH7* (type I) and *MYH2* (type IIA) genes that both decreased after atrophy and repeated
731 atrophy whereas fast *MYH1* (type IIX) increased after both periods of atrophy (**Figure 1N**). Overall,
732 suggesting a predominant downregulation of slow MYL and MYHC´s after repeated atrophy and an
733 increase in type IIX myosin, thus suggestive of a shift towards a faster phenotype in response to disuse.

Finally, expression of embryonic *MYH3* and perinatal *MYH8* both significantly increased after repeated atrophy (**Figure 1N**).

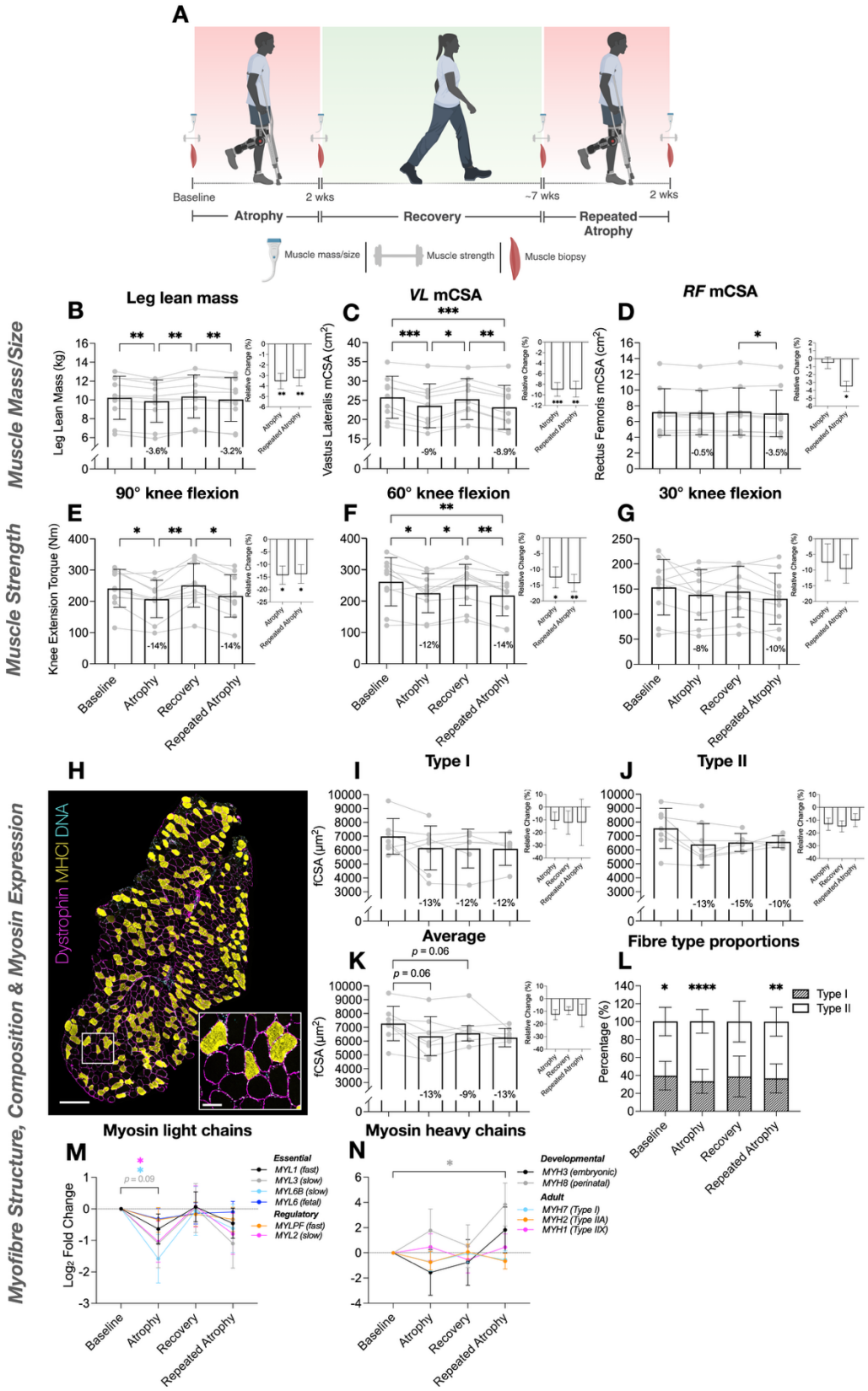

Figure 1. Young adult human intervention study design (created using BioRender.com) **(A).** Changes in leg lean mass **(B),** *Vastus Lateralis* (*VL*) mCSA **(C)**, *Rectus Femoris* (*RF)* mCSA **(D)** and strength/MVC across knee flexion angles 90, 60 and 30° **(E, F, G** respectively**)** after disuse (atrophy), recovery and repeated disuse (repeated atrophy). Significant reductions in muscle size and strength were observed after disuse atrophy, restored during recovery and reduced to a similar extent after repeated atrophy. *RF* mCSA only occurred after repeated disuse **(D).** Bar graphs depict relative change (%) from the previous timepoint (i.e., atrophy versus baseline, repeated atrophy versus recovery). *N* = 10 for leg lean mass **(A)** and strength **(E-J)**; *n* = 9 for mCSA (**B-D**). Myofibre analyses **(H-M)** revealed a non-significant reduction in fCSA **(H-K).** *N* = 8 baseline and atrophy, *n* = 6 recovery, *n* = 5 repeated atrophy. **(H)** Representative fluorescence microscopic image (10× magnification; magenta = dystrophin/myofibre membrane, yellow = MHCI/type I myofibres, cyan = DNA, non-staining = putative type II myofibres; Scale bar within tile scan image = 500 µm, scale bar within magnified inset image = 100 µm). FibeRtypeR[90] analysis suggested a larger proportion of fast/type II versus slow/type I fibres at baseline, atrophy and repeated atrophy with no significant differences at recovery (**L**). Despite no significant reduction in fCSA, there was reduced mRNA levels of slow isoform *MYL* and *MYH* genes after atrophy and repeated atrophy as well as increased fast type IIX (*MYH1*) and developmental *MYH* genes after repeated atrophy (**M & N**). *N* = 9 for each timepoint derived from RNA-seq data. $*p \leq 0.05$, $**p \leq 0.01$, $**p \leq 0.001$, $****p \leq 0.0001$.

Repeated TTX-induced disuse atrophy results in a reduction in dorsiflexor muscle mass and fibre cross-sectional area (fCSA) and a lack of recovery in aged rat muscle

In aged animals, there was no significant reduction in body weight in controls, atrophy or recovery animals (*p* = *N.S*) (**Supplementary Table 1**). However, a significant reduction in body weight after repeated atrophy (-18.1%, *p* = 0.02) as well as mean post-interventional versus pre-surgical body weight when pooling all conditions (-11.7%, *p* = 0.003, **Supplementary Table 1**). Thus, muscle weights were normalised to respective body weights for each condition throughout. TTX administration to the common peroneal nerve (CPN) (**Figure 2A**) resulted in a non-significant loss of TA muscle weight during initial atrophy (-4.4%, *p* = 0.6) and a significant loss after repeated TTX-induced atrophy (-29.8%, *p* = 0.002, **Figure 2B**). There was also a significant reduction in EDL muscle weight following repeated atrophy (-31.1%, *p* = 0.01). Previously published work by our group reported sufficient recovery of muscle mass following TTX-induced atrophy in young adult rats [66]. However, despite TTX-cessation and a return to normal dorsiflexion in aged rats during the recovery period, TA muscle loss continued to occur after recovery (-17.9%, *p* = 0.01, **Figure 2B**), despite shorter TTX exposure and longer active recovery than young adult rats [66]. There was no significant reduction in plantarflexor (soleus, plantaris and gastrocnemius) muscle weights, thus emphasising precise selective silencing of the dorsiflexor muscles using TTX to the common peroneal nerve (*p* = *N.S*, **Supplementary Figure 3A-D**). At the transcript level, there was increased expression of developmental myosin heavy chain (*Myh3/8)* genes across all conditions (**Figure 2C**), whereas adult fast (*Myh1/4*), slow (*Myh7*) myosin heavy chains, as well as essential (*Myl3*) and regulatory (*Mylpf/2*) myosin light chains significantly decreased after both periods of disuse (**Figure 2D**). Interestingly, these returned to control levels upon recovery despite continued muscle loss during TTX cessation (**Figures 2C & D**) suggesting that *Myh1/4/7* and *Myl2/3/pf* genes were sensitive to the TTX-disuse stimulus. Conversely, *Myh2*, *Myl1* and *Myl4* gene expression significantly increased following TTX cessation only. Overall, persistent elevation of developmental *Myh3* and *Myh8* mRNA expression coupled with significant reductions in adult fast and slow *Myh* and *Myl* isoforms occurred after both periods of atrophy. Coinciding with reductions in muscle weight and *Myh* and *Myl* expression, IHC analysis (**Figure 2E**) showed a significant loss in average (type I & II

combined, **Figures 2F & K**), type I (**Figures 2G & L**) and type IIA (**Figures 2H & M**) myofibre cross-sectional area (fCSA) after repeated atrophy. There was also a significant reduction in pure type I (**Figure 2G & L**) and hybrid I/IIA (**Figure 2I & N**) fCSA after initial TTX-induced atrophy, thus supporting the transcriptional expression data that slow fibres were sensitive to TTX-induced disuse. When relativising left TTX to right control limb, there were no significant changes in fCSA across all fibre types (**Supplementary Figures 3 F-J**). Finally, there was a greater contribution of type IIA and reduced proportion of IIX/IIB fibres after recovery (**Figure 2P**) as well as a leftward shift and larger frequency of smaller (≈ <1000 μm^2) predominantly slower fibres in the left TTX versus right control limb (**Figures 2Q-U**).

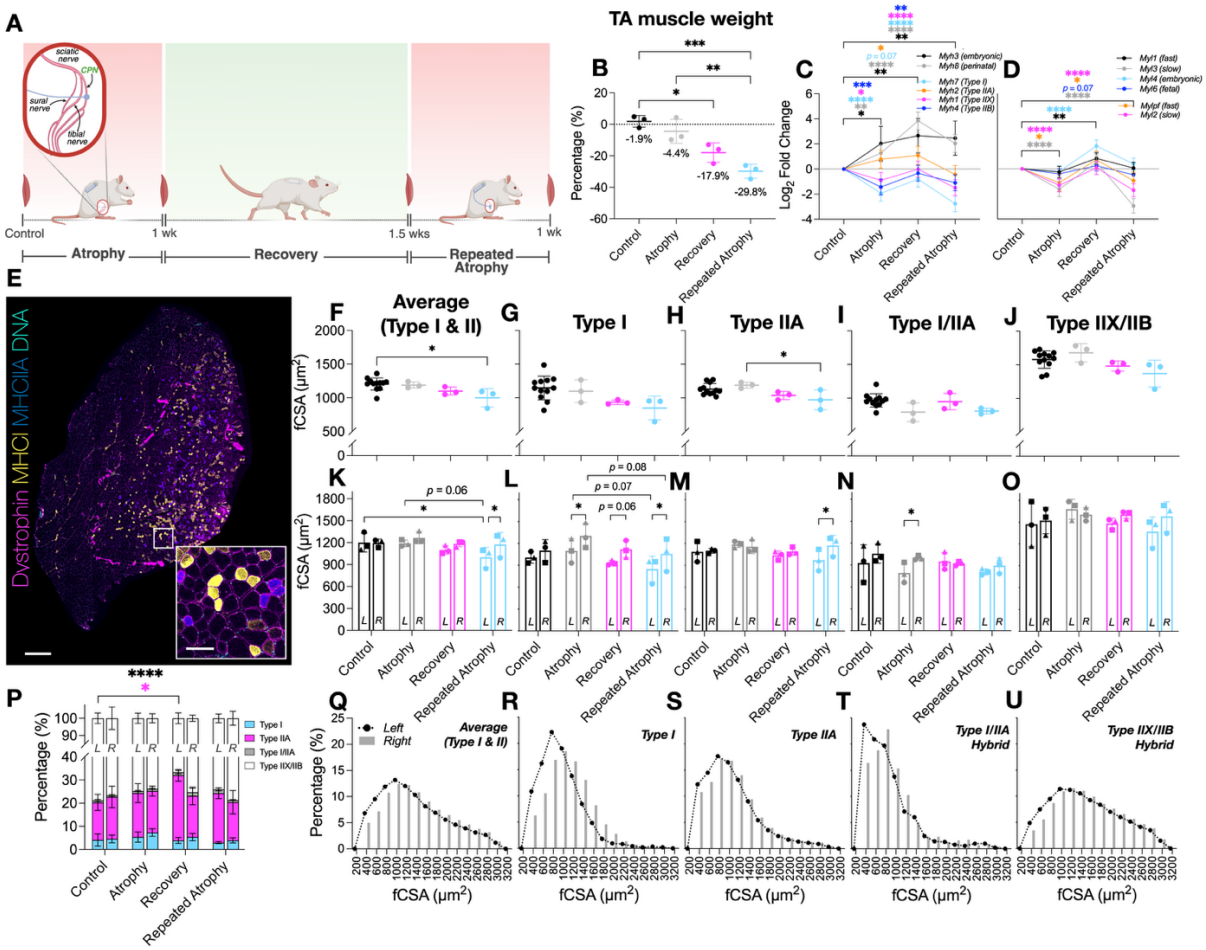

Figure 2. (**A**) Schematic representation of repeated disuse model in aged animals (created with BioRender.com). CPN = common peroneal nerve. (**B**) Reduction in TA muscle weight during atrophy and repeated atrophy with lack of recovery (presented as % change of the left TTX versus right control limb normalised to body weight). (**C**) Myosin heavy chain transcriptional analysis revealed significant changes in developmental (*Myh3/8*) and adult (*Myh7/2/1/4*) isoforms after atrophy and repeated atrophy (**D**) Essential (*Myl1/3/4/6*) and regulatory (*Mylpf/2*) myosin light chains were also differentially expressed after atrophy, recovery and/or repeated atrophy yet most were restored during recovery, despite continued muscle loss (**E**) Representative fluorescence microscopic image of whole TA muscle section labelled with dystrophin (magenta), MHCI (yellow), MHCIIA (blue), DNA (cyan). Non-staining represents putative type IIX/IIB myofibres. Tile scan images acquired at 10× magnification (scale bar within scan image = 500 μm, scale bar within magnified inset image = 100 μm). (**F-O**) There were significant reductions in fCSA of predominantly slow fibres after atrophy (pure type I and I/IIA hybrid fibres) and repeated atrophy (average, type I and IIA fibres). Symbol shapes represent individual animals. (**P**) Proportional fibre type analysis revealed greater contribution of type IIA and

802 reduced number of IIX/IIB after recovery versus control in the left surgical limb. (**Q-U**) Fibre size distribution analysis demonstrates
803 a leftward shift and larger frequency of smaller (<1000 μm^2) fibres in the left TTX versus right control limb. *$p \leq 0.05$, **$p \leq 0.01$,
804 ***$p \leq 0.001$. fCSA = myofibre cross-sectional area.
805
806 *Atrophy and repeated atrophy in adult human muscle predominantly alters transcript expression of*
807 *genes associated with aerobic metabolism, mitochondrial function, skeletal muscle structure and*
808 *function*
809
810 In young adult humans, the largest changes in gene expression occurred after initial atrophy, where
811 most genes were downregulated after both atrophy and repeated atrophy (**Figures 3A-F**). PCA analysis
812 revealed a larger overlap between baseline and recovery as well as between atrophy and repeated
813 atrophy timepoints, suggesting a closer transcriptomic profile between both periods of physical activity
814 (baseline and recovery) and inactivity (atrophy and repeated atrophy) (**Figure 3B**). Among the 15,096
815 genes detected, there were 4-5-fold more DEGs after initial atrophy (381 DEGs) than after repeated
816 atrophy (103 DEGs vs. baseline, 82 DEGs vs. recovery) with predominant downregulation of genes
817 after both atrophy (63%) and repeated atrophy (77% vs. baseline, 85% vs. recovery) (**Figures 3C-F**).
818 Following recovery from initial atrophy, more genes were upregulated (58%) (**Figure 3E**). Venn diagram
819 analysis demonstrated a large proportion of overlapping downregulated (45% of total repeated atrophy
820 DEGs vs. baseline and recovery) or upregulated (53%) genes after both periods of atrophy (**Figure**
821 **3G**). During recovery, there were no detected DEGs relative to baseline, with 536 DEGs following
822 recovery from initial atrophy which were all unique from atrophy and repeated atrophy comparisons
823 (**Figures 3E & G**).
824
825 Interrogation of the most differentially expressed genes across comparisons revealed that *NMRK2,* an
826 NAD^+ biosynthesis gene, was among the top-most downregulated DEGs after atrophy (-8.4 FC, FDR
827 most significant), ranked second to the nuclear receptor, *NR4A3* (-11.5 FC, **Figures 3C & H**). *NMRK2*
828 was also the most downregulated gene after repeated atrophy versus baseline (-5.0 FC) and when
829 compared with recovery (-5.6 FC), as well as the most upregulated DEG after recovery versus atrophy
830 (9.2 FC**, Figures 3C & H).** Interestingly, after repeated atrophy only, the most upregulated genes were
831 developmental myosin heavy chain *MYH8* (14.2 FC vs. baseline, 9.8 FC vs. recovery), tropomyosin-
832 binding subunit *TNNT2* (8.3 FC vs. recovery) and NMJ nicotinic acetylcholine receptor (nAChR) subunit
833 genes, *CHRNA1* (5.4 FC versus baseline) and *CHRND* (4.0 FC versus baseline) (**Figure 3D & F)**.
834 Another AchR subunit gene, *CHRNG* (2.86 FC versus baseline), was one of the most upregulated by
835 average FC (across all timepoints) only after repeated atrophy (**Figure 3H**).
836
837 Such transcriptional perturbations across the transcriptome corresponded to significant downregulation
838 of enriched pathway and gene ontology terms related to aerobic metabolism, respiration (e.g., NAD^+ /
839 NADH metabolism, TCA cycle, ETC, ATP synthesis) and mitochondrial structure, function and turnover
840 after both periods of disuse, with these genes returning to baseline levels after recovery (**Figures 3I &**
841 **J** and **Figure 3K, cluster 1).** Furthermore, enrichment of upregulated genes (including AchR subunits
842 and *MYH8 and TNNT2* highlighted above) were associated with muscle-specific terms including

843 acetylcholine receptor signalling, synaptic transmission, membrane depolarisation and skeletal muscle
844 contraction (**Figure 3I and J**).
845
846 *Young adult skeletal muscle demonstrates a transcriptional protection against repeated atrophy*
847
848 Temporal gene clustering analysis (SOM) revealed most genes decreased (57%, cluster 1) and
849 increased (41%, cluster 2) after atrophy, returned to baseline levels after recovery, and were less
850 susceptible to changes after repeated disuse (**Figure 3K**). This represents a transcriptional attenuation,
851 resulting in a smaller magnitude of change to repeated atrophy stimuli for both downregulated (cluster
852 1) and upregulated (cluster 2) genes. Based on SOM standardised means, there was a 40% smaller
853 magnitude in downregulation of genes in cluster 1 and an 72% smaller magnitude in upregulation of
854 genes in cluster 2 after repeated atrophy compared with initial atrophy. Enriched pathway and GO terms
855 associated with the response of these downregulated genes to both periods of disuse (cluster 1) were
856 the same aerobic metabolism, respiration and mitochondrial-related terms identified across global
857 downregulated genes described above (i.e. NAD^+ / NADH dehydrogenase activity, TCA cycle, ETC,
858 ATP synthesis and mitochondrial structure, assembly and protein turnover pathway genes, **Figures 3L**
859 **& M**). Genes that were upregulated after atrophy and increased less after repeated atrophy (cluster 2,
860 **Figure 3K**), were enriched in terms related to amino acid transport, transcription coregulator/coactivator
861 activity and chromatin binding (**Figure 3L & M**). In contrast, genes associated with these
862 terms/pathways were also downregulated during recovery from atrophy (**Figure 3J**). Therefore, the
863 fewer number of total DEGs coupled with less susceptible alterations to repeated versus initial atrophy
864 suggests a transcriptionally protective memory of earlier atrophy.
865
866 SOM cluster temporal analysis also identified 11 downregulated genes (*NR4A1, NR4A3, PRKAG2,*
867 *RP9, CIITA, CORO2B, ENSG00000242299, RPL35, SNRPA1, UBE3D, RPL29P11*) after atrophy that
868 remained downregulated during recovery, despite restoration of muscle mass (cluster 3, **Figure 3K**).
869 This included nuclear receptor genes, *NR4A1* and *NR4A3,* as well as *PRKAG2* (AMPK gamma2),
870 where *NR4A3* was among the top ranked downregulated genes within enriched metabolic processes.
871 Also, ribosomal genes (*RPL35, RPL29P11*) that also demonstrated downregulated enrichment at the
872 pathway/term level after atrophy (**Figure 3J**). Suggesting a memory of atrophy at the transcriptional
873 level in these genes via retention of gene expression changes from initial disuse even after the recovery
874 period.
875
876 Finally, 6 genes (*TNNT2, MYH3, DCLK1, ZBED6CL, CDC73, WDR44*) were upregulated after atrophy,
877 remained elevated during recovery, with even larger increases in expression after repeated atrophy
878 (cluster 4, **Figure 3K**). This included *TNNT2* (top ranked upregulated gene as discussed above),
879 embryonic myosin heavy chain (*MYH3*), *DLK1* associated with regeneration of muscle following injury,
880 and *ZBED6CL* also linked with muscle development. Therefore, whilst most genes demonstrated
881 transcriptional protection after repeated atrophy, a small number of genes related to muscle
882 development and regeneration (together with the AchR subunit genes discussed above) demonstrated

exaggerated responses to repeated atrophy in adult human muscle. The retained upregulation and exaggerated increases after repeated disuse also suggests a memory of earlier atrophy at the transcriptional level in these genes.

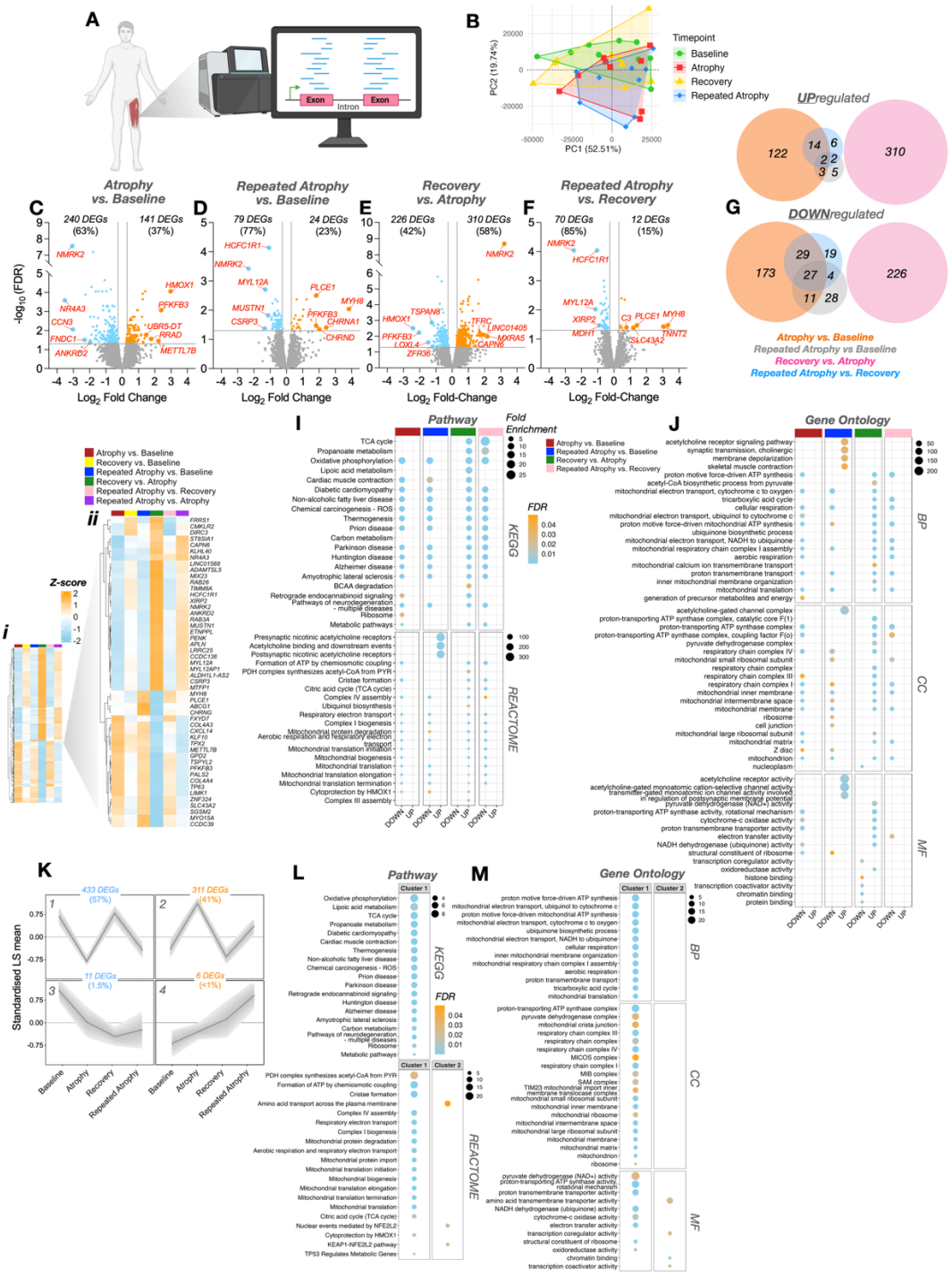

Figure 3. (**A**) Schematic depicting the transcriptomic response to repeated disuse atrophy in young adult human skeletal muscle (created with BioRender.com). (**B**) Principal component analysis (PCA) by time point. (**C-F**) Volcano plots depicting the number of differentially expressed genes (DEGs) that were either DOWN- (blue) or UP-regulated (orange) for each pairwise comparison. There were no detected DEGs (and thus no volcano plots) for "Recovery vs. Baseline" nor "Repeated Atrophy vs. Atrophy" comparisons. Labelled genes within volcano plots represent the top 5 DEGs according to greatest FC in either direction of change (FDR ≤ 0.05). (**G**) Venn diagrams depicting the number of unique and common DEGs across all timepoints for both DOWN- (bottom) and UP-regulated (top) DEGs. (**H**) Heatmap of all DEGs in at least one comparison (**i**). Magnified heatmap displaying

894 the top 25 DOWN- (blue) or UP-regulated (orange) genes according to average fold-change across all timepoints (**ii**). Over-
895 representation analysis (ORA) of the top 20 enriched (**J**) pathway (KEGG, top 4 panels; REACTOME, bottom 4 panels) and (**K**)
896 gene ontology (GO) terms for both DOWN- and UP-regulated DEGs across all comparisons ("Atrophy vs. Baseline", "Repeated
897 Atrophy vs. Baseline", "Recovery vs. Atrophy", "Repeated Atrophy vs. Recovery"). (**K**) Self-Organizing Maps (SOM) composed
898 of 761 genes that were significantly differentially expressed in at least one comparison, illustrating gene cluster temporal profiles
899 across the time-course of atrophy, recovery and repeated atrophy. Cluster 1 & 3 (blue) represent genes that were DOWN-
900 regulated following the first period of atrophy. Cluster 2 & 4 (orange) depict UP-regulated genes after initial atrophy. (**L**) Pathway
901 and (**M**) GO analysis revealed enriched terms for clusters 1 and 2 only, in which most genes were either DOWN- (Cluster 1) or
902 UP-regulated (Cluster 2) after atrophy, recovered upon reloading and were less susceptible to changes after repeated atrophy.
903 Cluster 3 represents downregulated genes after atrophy, with retained reduction during recovery and repeated atrophy. Cluster
904 4 represents upregulated genes after atrophy, retained during recovery, followed by greater increases in expression after
905 repeated atrophy. BP = biological process, CC = cellular component, MF = molecular function.
906
907 *Repeated atrophy in aged muscle results in downregulation of aerobic metabolism, NAD^+/NADH and*
908 *muscle-specific genes and upregulation of genes associated with ECM, protein turnover and DNA*
909 *damage*
910
911 Alongside the loss of TA muscle mass during atrophy, recovery and repeated atrophy in aged animals,
912 there were considerably large transcriptomic perturbations after atrophy and recovery with the greatest
913 changes detected after repeated atrophy (**Figures 4A-I**). PCA analysis showed similar clustering of
914 TTX-induced atrophy and repeated atrophy, and distinct clustering after TTX cessation-induced
915 recovery (**Figures 4B & C**). There was also considerable overlap of the sham surgical and pooled non-
916 surgical controls (**Figure 4B**). Given there were also no DEGs detected between sham and pooled
917 contralateral control limb samples, suggesting the surgery had no significant impact on gene
918 transcription, we excluded sham samples from further analysis and pooled contralateral (right) non-
919 surgical limb samples for the control group. Among the 11,284 genes detected post-normalization, there
920 was a similar number of DEGs in response to atrophy (2106 DEGs) and recovery (2008 DEGs) with 2-
921 fold more DEGs detected after repeated atrophy (3937 DEGs) vs. controls. The proportion of
922 downregulated DEGs was 56% after atrophy (**Figure 4D**), 53% after recovery and 56% (vs. control) or
923 58% (vs. recovery) after repeated atrophy (**Figure 4F-H)**. However, despite a similar number of total
924 DEGs after atrophy and recovery, the majority of downregulated (90%) and upregulated (74%) DEGs
925 were unique after TTX cessation (**Figure 4J**), as evidenced by the distinct PCA clustering of recovery
926 samples (**Figure 4C**). Also, whilst the 2-fold greater number of DEGs after repeated atrophy versus
927 initial atrophy may be partially explained by the lack of recovery during the no TTX period, when
928 relativised to previous recovery, the number of DEGs after repeated atrophy (3198 DEGs) was still 1.5-
929 fold more than initial atrophy (2016 DEGs) (**Figure 4H**), that corresponded to a -11.9% reduction in
930 muscle mass after repeated atrophy versus recovery (**Figure 2B**). There were 79 DEGs after repeated
931 versus initial atrophy in aged animals with a larger number of downregulated (84%) versus upregulated
932 (16%) genes (**Figure 4I)**. Most of these were shared across both periods of atrophy (2461 DEGs/75%
933 downregulated, 3935 DEGs/61% upregulated), but several downregulated (1294 DEGs/25%) and
934 upregulated (1550/39%) DEGs that were unique to repeated atrophy (**Figure 4J**).
935

936 Regarding gene-specific alterations, the top downregulated DEGs included genes associated with NMJ
937 function and stability (*Ache, Unc5a, Ntf3, Nfasc*), mitochondria and metabolism (*Park7, Perm1, Nfil3,*
938 *Gpd1, Acss1, Mc5r, Dhrs7c, G0s2, Fbp2*), muscle structure and contraction (*Lrrc38, Ky, Mylk2, Rgn*)
939 as well as DNA damage (*Fanca, Ddit4l2*) (**Figure 4K).** Interestingly, the myokine, *Apln*, important for
940 angiogenesis, muscle regeneration and ATP synthesis was among the top 5 downregulated genes after
941 initial TTX-induced atrophy (-9.7 FC, **Figure 4D**) (that also decreased after repeated atrophy) and was
942 within the top 25 downregulated genes in young adult humans after atrophy (**Figure 3H**). Concerning
943 the top upregulated genes, the muscle specific fuso-gene, *Mymk* significantly increased after both
944 atrophy (12.8 FC*,* **Figure 4D**) and repeated atrophy (18.6 FC, **Figure 4F**), implying satellite cell fusion
945 in attempt to repair and/or offset TTX-induced muscle wasting. Also, among the top-ranked upregulated
946 genes after initial atrophy was tropomyosin-binding, *Tnnt2* (11.8 FC*,* **Figure 4D)**. Embryonic *Myh8* was
947 one of the most upregulated DEGs after recovery (14.3 FC, **Figure 4E**) and was among the top-ranked
948 upregulated DEGs in young adult human muscle after repeated atrophy (**Figures 3D & F**). Further,
949 NMJ AChR subunit genes, *Chrnd,* and *Chrna1* were both ranked among the top upregulated genes in
950 aged animal muscle after both atrophy (*Chrnd* = 5.8 FC*, Chrna1* = 7 FC) and to a greater extent
951 repeated atrophy (*Chrnd* = 12.5 FC*; Chrna1* = 16 FC) whilst *Chrng* significantly increased only after
952 repeated atrophy (**Figure 4K**). Such AChR genes were also similarly upregulated in young adult human
953 muscle following disuse (**Figure 3D & H**). Collectively, genes *Tnnt2, Myh8, Chrna1, Chrnd* and *Chrng*,
954 increased in response to disuse-induced muscle wasting, irrespective of age, species and atrophy
955 model utilised.
956
957 Enrichment analysis of downregulated genes revealed similar pathways and GO terms after both
958 atrophy and repeated atrophy in aged muscle. Specifically, terms related to metabolic processes and
959 aerobic respiration (e.g., NAD binding / NADH dehydrogenase activity, TCA cycle, ETC and ATP
960 synthesis) as well as muscle-specific terms (e.g., muscle contraction, cytoskeleton in muscle cells and
961 sarcomere organisation) (**Figure 4L & M**). Such terms were also enriched in downregulated DEGs after
962 atrophy and repeated atrophy in young adult human muscle. In contrast, most of these terms were
963 enriched in upregulated DEGs during recovery from atrophy, suggesting they recovered after the initial
964 disuse, despite continued muscle wasting after TTX cessation. This suggests that genes were TTX-
965 sensitive during disuse rather than simply reflecting the continued muscle wasting observed during
966 recovery and a possible attempt to restore muscle during return to activity. This was also observed in
967 young adult human muscle, where expression of genes within these pathways, alongside skeletal
968 muscle size and strength, returned to baseline levels during recovery. Upregulated pathway enrichment
969 that occurred after both atrophy and repeated atrophy was evident within ribosomal structure and
970 subunit genes (**Figure 4L**). Interestingly, genes associated with proteasomal core and accessory
971 complex, ECM turnover, ubiquitin-mediated proteolysis and DNA damage pathways only increased
972 after repeated atrophy (**Figure 4L-M**).
973
974

975 *Aged muscle demonstrates an exaggerated transcriptional response following repeated atrophy in*
976 *genes that are fully restored during recovery*
977
978 Temporal clustering analysis by SOM profiling revealed the majority of genes that were downregulated
979 (40% cluster 3) or upregulated (35%, cluster 2) after atrophy, were restored to control levels after TTX
980 cessation during recovery, followed by exaggerated changes after repeated disuse (**Figure 4N**).
981 Specifically in cluster 3, downregulated genes after atrophy that returned to control levels during
982 recovery (despite continued loss of muscle mass), followed by greater reductions during repeated
983 atrophy, were enriched in: aerobic metabolism, TCA cycle, NAD binding/NADH dehydrogenase activity,
984 ETC and ATP synthesis in the mitochondria as well as in muscle structure and function (cluster 3)
985 (**Figures 4O & P**). Based on SOM standardised means, on average there was a 95% larger magnitude
986 of decreased expression of genes within cluster 3 after repeated atrophy compared with initial atrophy.
987 Therefore, genes in these metabolic pathways demonstrated, on average, a 95% more exaggerated
988 downregulation of transcripts in response to repeated atrophy, whereas young adult human muscle
989 demonstrated less susceptible attenuated transcriptional response in genes within the same pathways
990 following repeated atrophy. This suggests a negative, detrimental and exaggerated transcriptional
991 response to repeated atrophy in aged muscle. Importantly, these genes still recovered to control levels
992 during recovery, despite continued muscle wasting in aged animals. Therefore, the exaggerated
993 response to repeated atrophy in aged muscle was not simply due to the lack of recovery but rather an
994 exaggerated response to repeated atrophy having experienced earlier TTX-induced disuse atrophy.
995
996 Genes within cluster 2 (**Figure 4N**) that were upregulated after atrophy, returned to control levels during
997 recovery and were upregulated to a greater extent during repeated atrophy, were enriched in
998 proteosome, ECM turnover, and DNA damage pathways in aged muscle. Based on SOM standardised
999 means, there was an average 141% larger magnitude in upregulation of genes in cluster 2 after
1000 repeated atrophy compared to the initial atrophy. These genes/terms were unique to aged muscle, also
1001 demonstrating recovery of gene expression despite continued muscle wasting during the recovery
1002 period, followed by exaggerated transcriptional and physiological responses to repeated atrophy.
1003
1004 A proportion of genes also decreased (11%, cluster 1) or increased (14%, cluster 4) to a lesser extent
1005 during atrophy with the largest change occurring during recovery, followed by a return to atrophy levels
1006 during repeated atrophy (**Figure 4N**). Genes in both clusters 1 & 4 were enriched in inflammatory
1007 pathways, ECM turnover, collagen assembly and matrix organisation (**Figure 4O & P**), suggestive that
1008 changes in inflammatory and ECM genes were associated with continued muscle wasting in aged
1009 muscle, despite TTX cessation.
1010

Figure 4. (**A**) Schematic depicting transcriptomic (via RNA-seq) analysis of repeated TTX-induced disuse atrophy in aged animals (created using BioRender.com). Principal component analysis (PCA) including (**B**) and excluding (**C**) sham surgery group. (**D-I**) Volcano plots depicting the number of differentially expressed genes (DEGs) that were either DOWN- (blue) or UP-regulated (orange) for each pairwise comparison. Labelled genes within volcano plots represent the top 5 DEGs according to greatest fold-change with FDR ≤ 0.05. There were no DEGs detected in sham versus pooled contralateral control limb, suggesting the surgery had no significant impact on gene transcription. The sham group was therefore excluded for all downstream analyses and pooled contralateral limb was used as the control. (**J**) Heatmap of all DEGs in at least one comparison (***i***). Magnified heatmap displaying the top 50 DOWN- (blue) and top 50 UP-regulated (orange) genes (by gene symbol) by average fold-change across all pairwise comparisons (***ii***). (**K**) Venn diagrams depicting the number of unique and common DEGs across all conditions for both UP- (top) and DOWN-regulated (bottom) DEGs. Over-representation analysis (ORA) of the top 20 enriched (**L**) pathway (KEGG, top 4 panels; REACTOME, bottom 4 panels) and (**M**) gene ontology (GO) terms for both DOWN- and UP-regulated DEGs across all comparisons ("Atrophy vs. Control", "Recovery vs. Control", "Repeated Atrophy vs. Control", "Recovery vs. Atrophy", "Repeated Atrophy vs. Recovery"). (**N**) Self-Organizing Maps (SOM) composed of a total 6379 genes that were DEGs in at least one comparison, illustrating gene cluster temporal profiles across the time-course of repeated disuse atrophy. Profiles 1 & 3 represent genes that were DOWN-regulated following the first period of atrophy whereas profiles 2 & 4 depict UP-regulated genes after initial atrophy. (**L**) Pathway and (**M**) GO analysis revealed enriched terms across all cluster profiles where most genes were

either UP- (cluster 2) or DOWN-regulated (cluster 3) after atrophy, recovered upon TTX cessation, followed by larger/exaggerated changes (in the same direction of initial atrophy) after repeated disuse atrophy. BP = biological process, CC = cellular component, MF = molecular function.

Young adult rat skeletal muscle recovers from TTX-induced atrophy after longer TTX exposure and shorter active recovery than aged rats herein

In both young adult human and aged rat muscle, initial and repeated atrophy both resulted in downregulation of genes associated with aerobic respiration and mitochondria terms. During return to habitual activity however, these pathways recovered both in young adult humans and in aged rat muscle, despite differential physiological responses. Given the optimal recovery observed in young adult humans and the lack of recovery in aged animals, we compared the physiological and transcriptomic response of aged rats to young adult rat muscle using the same TTX-induced atrophy and recovery model [66]. Previously published work by our group reported sufficient recovery of muscle mass following TTX-induced atrophy despite longer TTX exposure and shorter active recovery [66]. Specifically, young adult rats received 2 wks of TTX exposure to the common peroneal nerve (versus 1 wk in aged rats in the present study), resulting in an average -51% and -69% loss of TA muscle mass and fCSA, respectively (**Figures 5A, B & C**). Interestingly, 1 wk active recovery (versus 1.5 wks in aged animals) recovered TA mass and fCSA by 53 and 63%, respectively relative to the previous 2 wks atrophy period (**Figures 5A & C**). This physiological response contrasts with aged animals herein, where TA muscle weight and fCSA continued to decrease during a longer active recovery, despite less atrophy observed following shorter TTX exposure (**Figures 5B-C**). Together with similar recovery of genes within the same pathways in young adult human muscle and aged rat muscle, this suggests that the lack of recovery in aged animals is dependent on age and not insufficient time to recover. In support of this, overlapping transcriptome datasets from young and aged animals revealed a considerable degree of overlap of DEGs after atrophy (77% upregulated and 72% downregulated DEGs) with a much smaller overlap after recovery (34% upregulated and 26% downregulated) (**Figures 5D-H**).

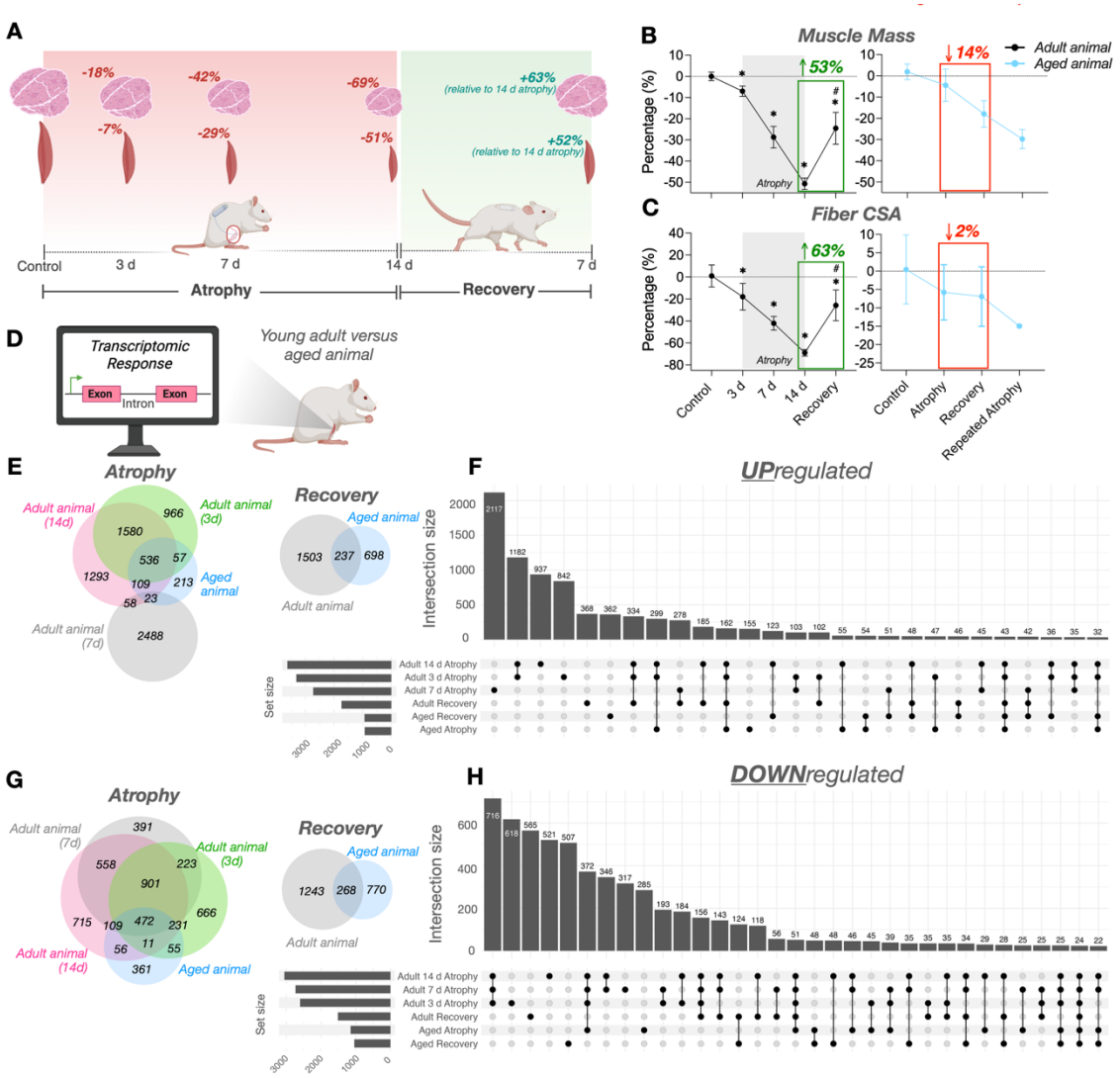

Figure 5. (**A**) Schematic of study design (created using BioRender.com) of TTX-induced atrophy (3, 7 and 14 days/d) and subsequent recovery (7 d) in young adult rats (Fisher et al.,) [66]. There was a loss of TA muscle mass (**B**) and fCSA (**C**) at 3, 7 and 14 d atrophy (-7 to -18%, -29 to -42% and -51 to -69%, respectively). In contrast to aged animals, muscle mass and fCSA was restored by 53 and 63%, respectively following 7 d recovery in young adult animals (**B & C** redrawn from Fisher et al., [66]). (**D**) Overlap of transcriptome in young adult and aged rat muscle revealed many common UP- (**E & F**) and DOWN-regulated (**G & H)** DEGs after atrophy and a larger proportion of unique genes after recovery.

Integrative DNA methylome and transcriptome analysis reveals epigenetically regulated gene expression after repeated atrophy related to NAD$^+$ metabolism, aerobic metabolism and mitochondrial structure & protein turnover pathways as well as NMJ genes

Retained and enhanced transcriptional responses to repeated hypertrophic stimuli have been associated with sustained DNA methylation alterations, thus proposing an important mechanism of muscle memory. Therefore, we next determine whether detected DEGs after atrophy, recovery and repeated atrophy were also associated with alterations in DNA methylation. Therefore, we performed DNA methylome analysis in both young adult human and aged animal skeletal muscle in response to atrophy, recovery and repeated atrophy and integrated these data with the transcriptome datasets described above. Repeated periods of disuse atrophy and recovery led to differentially methylated DNA

1070 regions (DMRs) that were inversely associated with the DEGs identified in both young (**Figures 6A-D**)
1071 and aged (**Figures 6E-H**) skeletal muscle. These genes are termed **D**ifferentially **m**ethylated **DEGs**
1072 (DmDEGs). In young adult humans, 71 DMRs on 57 genes (from cluster 1 above, **Figure 3K**) were
1073 identified as DmDEGs with an inverse relationship of hypermethylation and decreased expression.
1074 These DmDEGs were hypermethylated and downregulated after atrophy and repeated atrophy, with
1075 both DNA methylation and gene expression returning to baseline levels after recovery where skeletal
1076 muscle was restored (cluster 1, **Figures 6B*i* & C*i***). ORA analysis identified these DmDEGs as enriched
1077 in NAD^+ metabolism, ETC, ATP synthesis, mitochondrial structure and mitochondrial ribosome
1078 pathways, demonstrating that the enriched terms of genes within cluster 1 of the transcriptomic analysis
1079 above (downregulated with atrophy, return to baseline levels during recovery and less susceptible
1080 changes during repeated atrophy, **Figure 3K**) were also epigenetically regulated in response to disuse
1081 atrophy and repeated atrophy. Of note, *NMRK,2* a gene involved in NAD^+ biosynthesis was among the
1082 top downregulated gene after both periods of disuse in young adult humans), was among the
1083 epigenetically regulated genes in this profile. Specifically, *NMRK2* was hypermethylated and
1084 downregulated during both periods of atrophy and was hypomethylated with increased transcription
1085 towards baseline levels during recovery. In addition to these hypermethylated and downregulated
1086 genes, there were 189 DMRs on 101 genes that were hypomethylated and upregulated after both
1087 atrophy and repeated atrophy (cluster 2, **Figures 6B*ii* & C*ii* & *Ciii***). There was no significantly enriched
1088 pathway or GO terms for this cluster, thus suggestive that most of these genes likely have divergent
1089 molecular, cellular and biological roles. However, several interesting hypomethylated and upregulated
1090 genes emerged from this cluster. Specifically, the AChR genes, *CHRND* and *CHRNA1* (that were
1091 upregulated after atrophy and/or repeated atrophy across both human and rat muscle transcriptomes,
1092 **Figure 3D-H**), demonstrated the largest hypomethylation and increased expression after repeated
1093 atrophy (**Figures 6B*ii* and C*ii***). These genes were among the few DmDEGs in young human muscle
1094 that demonstrated increased susceptibility and exaggerated responses to repeated atrophy. Finally,
1095 genes *NR4A1* and *PRKAG2* (AMPK gamma2) were downregulated after atrophy (despite no change in
1096 DNA methylation) followed by hypermethylation and sustained suppression of transcription during
1097 recovery and repeated atrophy (cluster 3, **Figure 6B*iii***). Thus, suggestive that the retained reductions
1098 in expression of these genes during recovery is likely due to associated hypermethylation, despite
1099 restoration of skeletal muscle upon returning to habitual activity. The full DNA methylome data to
1100 repeated atrophy in young adult human muscle is also available in the supplementary files
1101 (**Supplementary Figure 4).**
1102
1103 In aged rat muscle, integrative analysis of DNA methylome and transcriptome (**Figure 6E**) revealed 41
1104 DMRs on 33 unique genes were hypermethylated and downregulated after atrophy (cluster 1, **Figure**
1105 **6Fi & Gi**), hypomethylated and upregulated upon TTX cessation during the recovery period, and finally
1106 hypermethylated and downregulated after repeated atrophy. As with the young human muscle, these
1107 genes were associated with aerobic metabolism/respiration, electron transport and mitochondrial
1108 components (**Figure 6H**). Integrative analysis also revealed 40 DMRs on 28 unique genes (cluster 2,
1109 **Figure 6Fii and 6Gii**) that were hypomethylated and upregulated after atrophy, hypermethylated after

1110 recovery, and hypomethylated and upregulated again after repeated atrophy. ORA analysis revealed
1111 no significantly enriched pathways or GO terms for this cluster. There were also 26 DMRs on 19 unique
1112 genes (cluster 3, **Figure 6Fiii & Giii**) that were hypermethylated and downregulated after atrophy,
1113 hypermethylated yet upregulated during recovery, and hypomethylated and upregulated after repeated
1114 atrophy, with no significantly enriched pathways or GO terms. Interestingly, 43 DMRs on 21 unique
1115 genes (cluster 4, **Figure 6F*iv & Giv)*** demonstrated hypermethylation and downregulation after atrophy,
1116 with retained hypermethylation and a continued decrease in gene expression during recovery, followed
1117 by subsequent hypomethylation and increased gene expression after repeated atrophy. These genes
1118 were enriched in JAK-STAT signalling genes (cluster 4, **Figure 6H**) and therefore demonstrated
1119 retained epigenetic and transcriptional signatures after the initial atrophy that were retained during
1120 recovery yet were oppositely hypomethylated and upregulated after repeated atrophy.
1121
1122 Despite the differential physiological response to repeated atrophy and recovery, both young adult
1123 humans (cluster 1, **Figures 6B*i,* C*i*, D)** and aged animals (cluster 1, **Figure 6F*i*, G*i*, H**) demonstrated
1124 associated DNA methylation and gene transcription of genes enriched within the same pathway and
1125 GO terms related to aerobic metabolism/respiration, electron transport and mitochondria (**Figures 6D**
1126 **& H**). However, the majority of these DmDEGs were specific to young human or aged rat muscle
1127 (**Figure 6I**), despite enrichment of the same metabolic pathways across species and models of atrophy
1128 (**Figure 6J**). Further cross-species comparison of the shared transcriptomic and epigenetic responses
1129 to repeated disuse in young adult human and age animal muscle via UpSet plots (**Supplementary**
1130 **Figure 5**), identified several common up (**Supplementary Figure 5A**) and downregulated DEGs
1131 (**Supplementary Figure 5B**) as well as hypo- (**Supplementary Figure 5C**) and hyper-methylated
1132 DMRs (**Supplementary Figure 5D**). It was also apparent that out of the 761 DEGs used for the SOM
1133 temporal profiling in human muscle, 54% (414 out of 761) of the genes were also differentially
1134 expressed in the aged rat muscle (**Supplementary Figure 5E**). Pathway (**Supplementary Figure 5F**)
1135 and GO (**Supplementary Figure 5G**) analyses suggested these shared genes were also related to
1136 oxidative metabolism, NAD^+, TCA cycle, ETC, ATP synthesis and mitochondrial function. Among these
1137 shared DEGs, there were 406 DMRs on 189 shared DEGs in young adult human muscle
1138 (**Supplementary Figure 5H)** that were associated with oxidative metabolism, ETC, ATP synthesis and
1139 mitochondria (**Supplementary Figure 5I & J**). In aged animals, these there were 56 DMRs on 16
1140 shared DEGs (**Supplementary Figure 5K**) that were related to mitochondria and RNA splicing
1141 (**Supplementary Figure 5L**). Overall, these data demonstrate epigenetic regulation of shared genes
1142 associated with oxidative metabolism across species in response to atrophy, recovery and repeated
1143 atrophy. The full DNA methylome data to repeated atrophy in aged rat muscle is also available as
1144 supplementary information (**Supplementary Figure 6).**

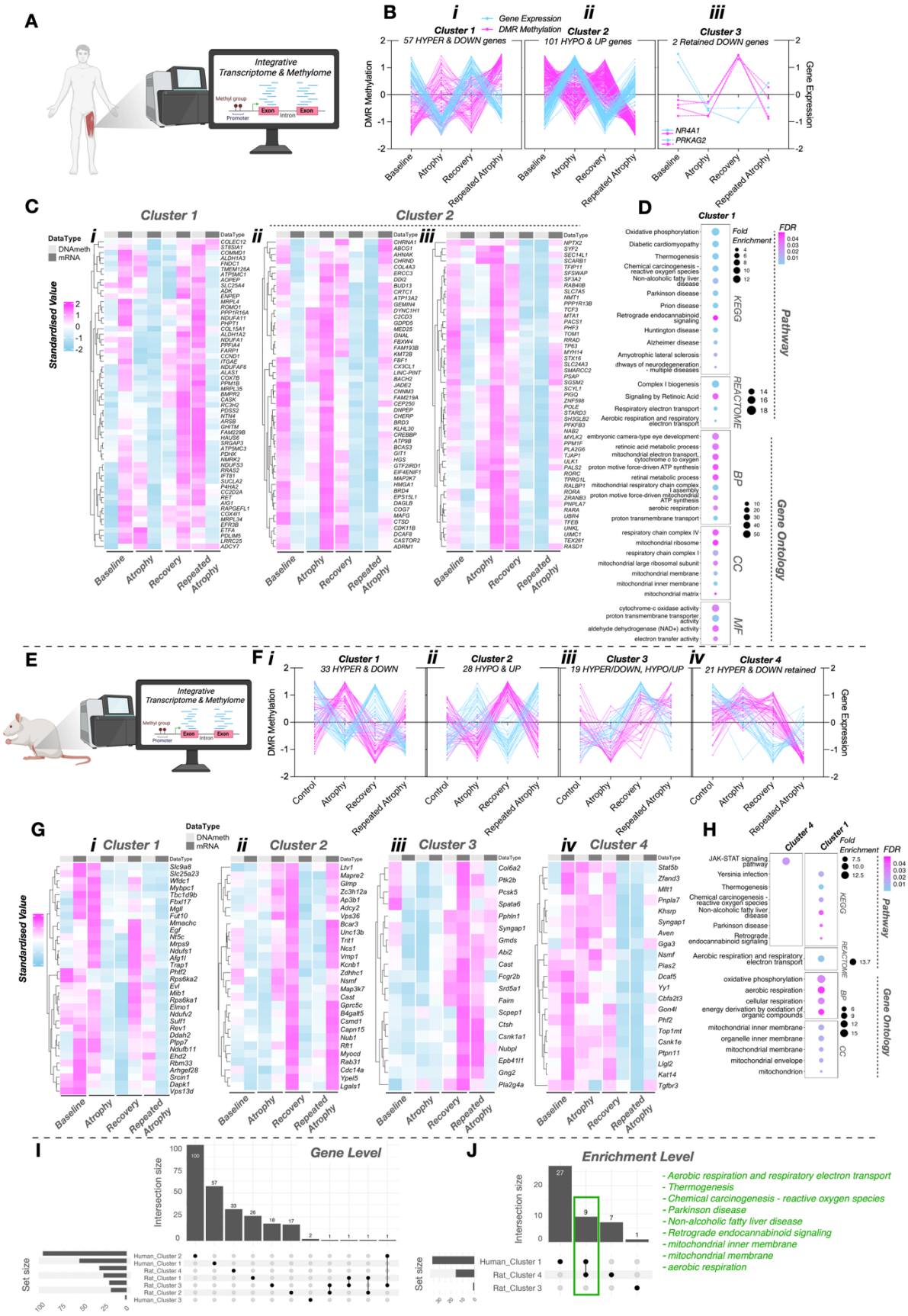

Figure 6. Integrative DNA methylome and transcriptome analyses in young adult human (**A-D**) identified 57 hypermethylated and downregulated genes after both periods of disuse that were returned to baseline levels after recovery (cluster 1, **Bi & Ci**); 101 hypomethylated and upregulated genes after both periods of disuse that also returned to baseline levels after recovery (cluster

2, **Bii & Cii**); 2 downregulated/hypermethylated genes after initial atrophy that were retained during recovery (cluster 3, **Biii & Ciii**). There were significant pathway and GO terms for cluster 1 in young human muscle of hypermethylated/downregulated genes after atrophy, restored during recovery, and hypermethylated/downregulated after repeated atrophy enriched in aerobic metabolism/respiration, NAD^+ activity, ETC, ATP synthesis, mitochondrial and ribosome terms (**D**). Integrative analyses in aged rat muscle (**E-G**) revealed 33 genes (**Fi & Gi,** cluster 1) hypermethylated/downregulated after atrophy, hypomethylated/upregulated upon TTX cessation during recovery, and hypermethylated/downregulated after repeated atrophy; 28 unique genes (**Fii & Gii,** cluster 2) were hypomethylated/upregulated after atrophy, hypermethylated/restored after recovery, and hypomethylated/upregulated again after repeated atrophy (**Fiii & Giii,** cluster 2); 19 unique genes (cluster 3) that were hypermethylated/downregulated after atrophy, hypermethylated yet upregulated during recovery, and hypomethylated/upregulated after repeated atrophy; 21 unique genes (**Fiv and Giv,** cluster 4) were hypermethylated/downregulated after atrophy, with retained hypermethylation and a continued decrease in gene expression during recovery followed by subsequent hypomethylation and increased gene expression after repeated atrophy. Significant enriched pathway and GO terms (**H**) for cluster 1 were related to aerobic metabolism/respiration, electron transport and specifically mitochondrial structure (for cluster 1) and JAK-STAT enrichment (in cluster 4). Average DMR methylation is depicted in aged animal heatmaps whenever there is >1 DMR for a given gene (**G**). Average mRNA expression is also presented where there were multiple transcript variants (**G**). UpSet plot analysis of young adult human and aged rat muscle gene clusters revealed only a few epigenetically regulated genes that overlapped between both models (**I**). However, there were 9 overlapping enriched pathway / GO terms between human and animal muscle (**J**). Note that 'DMR Methylation' is standardised percentage DMR methylation derived from SOM profiling analysis and 'Gene Expression' is representative of standardised LS means from SOM profiling analysis (**B & F**). BP = biological process, CC = cellular component, MF = molecular function.

Repeated atrophy in aged muscle leads to significant transcriptional perturbations of NAD+ biosynthesis genes resulting in reduced NAD+ content

Genes associated with NAD/NADH metabolism were enriched as downregulated and hypermethylated after atrophy and repeated atrophy in both young adult (**Figure 7A-D)** and aged rat (**Figure 7E-I**) muscle. Moreover, the NAD^+ biosynthetic gene, *NMRK2,* was the among the top downregulated genes after both periods of atrophy with inversely associated DNA across the time course of atrophy, recovery and repeated atrophy. Genes enriched in these pathways were also restored during the recovery period. Targeted mRNA analysis (via qPCR) of *Nmrk2* in aged rat muscle revealed a non-significant reduction in *Nmrk2* expression after atrophy, followed by a significant increase during recovery and a larger significant reduction after repeated atrophy (**Figure 7E & G**). Given the predominant role of *NMRK2/Nmrk2* in synthesising NAD^+ coupled with over-representation of NAD/NADH metabolism related enrichment terms for downregulated genes during both periods of atrophy, we next interrogated gene expression of other NAD^+ biosynthesis genes and whether such alterations corresponded with a reduction in NAD^+ content in both young adult (**Figure 7A-D**) and aged muscle (**Figure 7E-I**). In young adult humans, while most of these NAD^+ genes were downregulated after both periods of atrophy, *NMRK2* was the only significantly downregulated DEG out of the 18 genes analysed (**Figures 7A-C**). Furthermore, *NMRK2* was the most upregulated gene across all DEGs after recovery from atrophy in humans (**Figure 3E**) and was among the identified DmDEGs that was downregulated less after repeated versus initial atrophy. Given *NMRK2* was the only significantly downregulated NAD^+ gene, this resulted in no significant changes in NAD^+ content (**Figure 7D**). In contrast, half of the 14 NAD^+ genes assessed in aged animals were significantly differentially expressed where most genes were downregulated after atrophy, either unchanged/restored or increased after recovery, followed by greater

1193 downregulation after repeated atrophy (**Figure 7E-G**), thus resulting in significantly reduced absolute
1194 NAD^+ content in the left (L) TTX versus right (R) control limb after repeated atrophy (**Figure 7H & I**).
1195
1196 *Human post-atrophy MuSC display greater differentiation capacity, responsiveness to NR*
1197 *supplementation as well as lower mtDNA content relative to pre-atrophy MuSC*
1198
1199 Given *NMRK2* was among the top downregulated genes after atrophy and repeated atrophy in humans,
1200 and is phosphorylated (and thus activated) by the vitamin B_3 derivative, nicotinamide riboside (NR), we
1201 next supplemented muscle derived cells (MuSC) derived from pre- and post-atrophy human biopsies
1202 with NR in an attempt to restore potentially impaired *NMRK1/2* expression and myogenesis *in vitro*
1203 (**Figure 7J-M**). Although *Nmrk2* expression and NAD^+ content was significantly decreased after disuse
1204 in aged animals, we could not isolate MuSC to perform such experiments in aged muscle. Similar
1205 proportions of myoblast (desmin+) to fibroblasts (TE7+) were observed between pre- and post-atrophy
1206 MuSC, thus negating possible effects of cell populations (**Figure 7L**). Despite limited myotube formation
1207 in the MuSC, likely due to a higher proportion of fibroblasts (≈ 60%) versus myoblasts (≈ 60%) (**Figures**
1208 **7K & L**), post-atrophy MuSC were more responsive to NR supplementation, where myotube size
1209 significantly increased in NR treated post-atrophy cells when compared to 7d differentiation (p = 0.03,
1210 **Figure 7M**). This was supported by lower *MYOD (early differentiation)* and greater *MYOG*
1211 *(fusion/differentiation)* gene expression in NR-supplemented MuSC, coupled with greater (albeit non-
1212 significant *NMRK1* and *NMRK2* expression (**Figures 7N-Q**). Interestingly, mtDNA content
1213 demonstrated lower mean (albeit non-significant) mtDNA in post- versus pre-atrophy MuSC (**Figures**
1214 **7R-U**). Collectively, post-atrophy MuSC were more responsive to NR supplementation that altered
1215 *NMRK* and *MYOG* expression and increased myotube size.
1216
1217

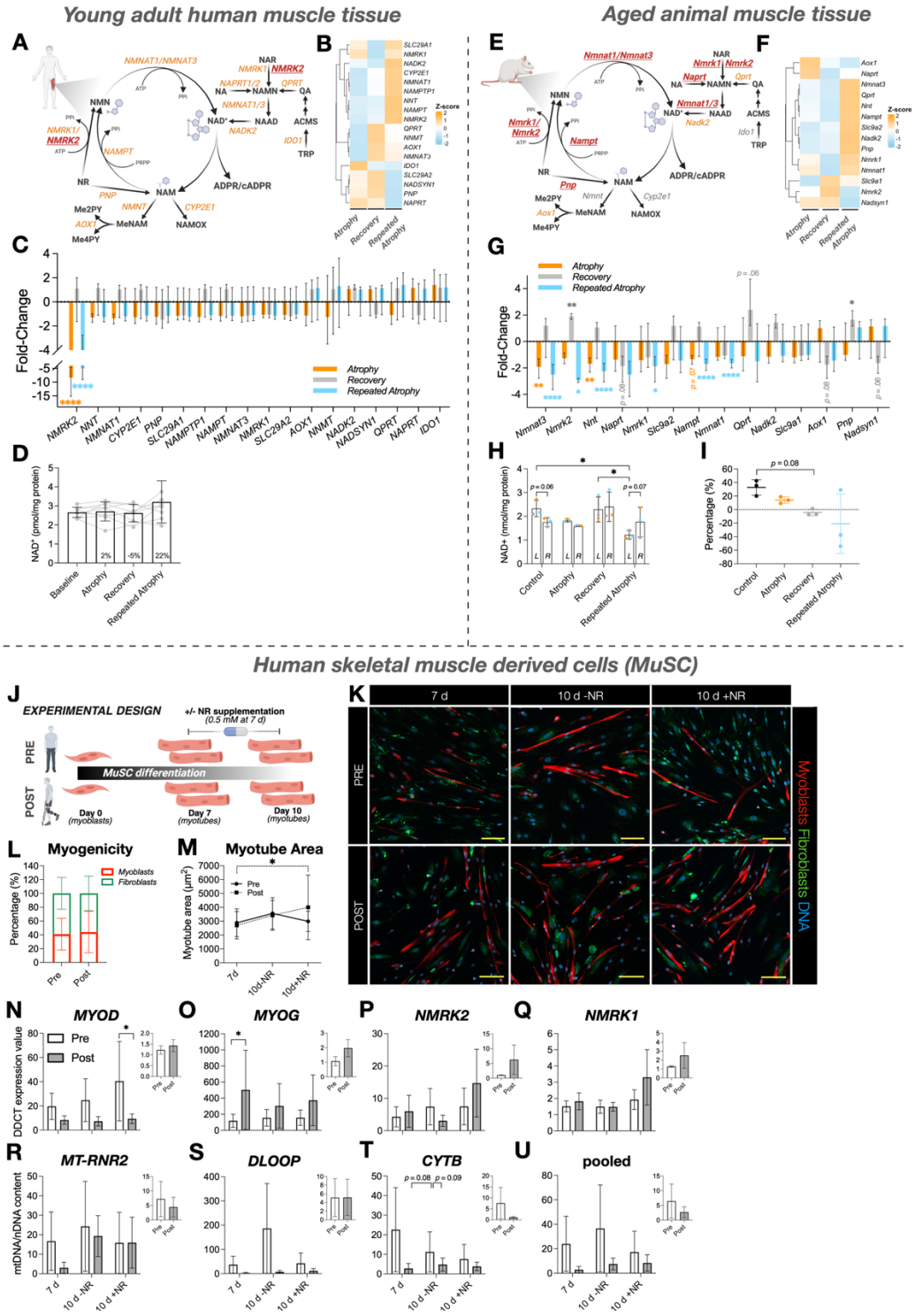

Figure 7. mRNA expression of NAD⁺ biosynthesis genes and corresponding NAD⁺ content in young adult human (**A-D**) and aged rat (**E-I**) skeletal muscle. (**A & E**) Schematic representation of Preiss-Handler and salvage NAD⁺ biosynthetic pathways (redrawn from Damgaard & Treebak, 2023 [91] using BioRender.com). Key metabolites are depicted as black text. Genes encoding NAD⁺ biosynthesis enzymes are shown in either orange (if non significantly expressed) or red text (significantly downregulated after atrophy or repeated atrophy). In young adult humans, *NMRK2* was the only significantly downregulated DEG out of the 18 NAD⁺ genes (**B & C**), which did not lead to significant alterations in NAD⁺ content (**D**). In aged animals, most of the 14 NAD+ genes assessed were significantly differentially expressed after atrophy and repeated atrophy and were restored upon recovery (**F & G**), resulting in significantly reduced absolute (**H**) NAD⁺ content in the left (L) TTX versus right (R) control limb after repeated atrophy. Relative NAD⁺ content (**I**). Nicotinamide riboside (NR) supplementation (0.5 mM) in human pre- and post-atrophy MuSC (n = 4) (J-K). (**K**) Fluorescence microscopic tile scan (3 × 3) images of MuSC labelled for myoblasts (desmin, red), fibroblasts (TE-7, green) and DNA (DAPI, blue), acquired at 10× magnification (scale bar = 200 µm). (**L**) Myoblasts (≈ 40%) and fibroblast (≈ 60%) proportions were similar between pre- and post-atrophy MuSC. NR supplementation resulted in significantly increased myotube area at 10 versus 7 d (p = 0.03) in post-atrophy MuSC only (**M**).

qPCR analysis revealed greater *MYOD* expression in pre-atrophy 10 d NR treated MuSC (**N**) coupled with greater *MYOG* expression at 7 d post-atrophy with no effect of NR treatment (**O**). Despite greater average *NMRK2* (**P**) and *NMRK1* (**Q**) expression in 10 d NR supplemented post-atrophy MuSC, this was not significantly different from pre-atrophy or non-treated MuSC. (**R-U**) There was a trend towards lower mtDNA content in post- versus pre-atrophy MuSC at each timepoint/condition, as well as lower mtDNA in NR treated pre-atrophy MuSC only, albeit not statistically significant. Larger main figures relativised to 0 h, small inset figures represent 10 d NR treated relativised to 10 d non-treated MuSC. *$p \leq 0.05$, **$p \leq 0.01$, ***$p \leq 0.001$, ****$p \leq 0.0001$. Myogenicity (**L**) and myotube area (**M**) data presented as mean ± SD. Gene expression (**N-Q**) and mtDNA (**R-U**) data presented as mean ± standard error of the mean (SEM).

Mitochondrial gene expression and DNA content is significantly impaired after repeated atrophy in young adult human muscle which is exacerbated in aged animal muscle

In addition to enrichment of NAD/NADH metabolism related genes, the majority of genes were also associated with mitochondrial structure, function, assembly and turnover in both young adult human and rodent muscle. Specifically, genes involved in aerobic respiration (and thus ETC and oxidative phosphorylation) and mitochondrial structural components were hypermethylated and downregulated after both periods of atrophy, with the majority of these genes returning to baseline levels in both human and rat muscle, despite restoration of muscle in humans and continued wasting in aged rats. Furthermore, these genes demonstrated further reductions in transcription in aged rat muscle, whereas these genes were less susceptible to reductions in young adult human muscle following repeated disuse. Given these data, we next assessed gene expression of mitochondrial fission, fusion, transport and biogenesis genes-specific genes, as well as mRNA and protein abundance of ETC protein complexes I-V. Finally, we assessed mtDNA copy number and citrate synthase protein abundance as markers of mitochondrial content/density. In young adult human muscle (**Figure 8A**), the majority of the 66 genes profiled across ETC complexes I-V were significantly suppressed after both periods of atrophy where most genes either returned to baseline levels or increased after recovery (**Figure 8B**). This resulted in significant changes occurring after both atrophy and repeated atrophy in 24 (out of 66) ETC genes; within complex I (7 out of 32 genes), III (3 out of 8 genes), IV (8 out of 13 genes), and V (6 out of 9 genes) with non-significant changes in CII (**Figure 8B**). Concerning genes related to mitochondrial fission and mitophagy (*FIS1, DRP1*), fusion (*MFN1/2, OPA1*), transport (*SLC25A51, SLC25A4)* and biogenesis (*PPARGC1A, TFAM*), 8 out of 9 of these genes non-significantly decreased after atrophy and repeated atrophy, all of which returned to baseline levels or non-significantly increased after recovery (**Figure 8C**). There was a significant reduction in *PPIF*, a mitochondrial membrane gene controlling calcium overload and fatigue resistance in muscle (**Figure 8C**). Given the large transcriptional perturbations in ETC-specific genes across all 5 complexes in both atrophy periods, we next assessed ETC (I-V) protein abundance. The reductions in gene expression did not correspond to significant changes in ETC protein complex abundance (**Figure 8D**). Interestingly however, mtDNA content (**Figure 8E**) and citrate synthase protein abundance (**Figure 8F**) significantly decreased after repeated atrophy only in young adult humans. Collectively, these data suggest that the large transcriptional perturbations of genes enriched in mitochondrial-specific pathways and GO terms culminated in impaired mitochondrial content and density following repeated disuse only in young adults despite restoration of these parameters and skeletal muscle during recovery.

1272 In aged animals, most genes across all ETC complexes were differentially expressed (**Figure 8H & I**).
1273 Specifically, 57% (38 out of 67) of genes encoding complex´s I (13 out of 30), II (4 out of 4), III (7 out of
1274 9), IV (6 out of 14) and V (8 out of 10 genes) were significantly downregulated after atrophy and/or
1275 repeated atrophy (**Figure 8H & I**). Similarly to young adult humans, the majority of these genes
1276 recovered during TTX cessation despite continued loss wasting during return to activity. Furthermore,
1277 *Sdhb, Cox6a1, Cox8a and Atp5pf* were significantly upregulated during recovery (**Figure 8I**). In contrast
1278 to young adult humans, aged rat muscle demonstrated a greater average reduction across all 67 genes
1279 following repeated atrophy (-1.72 FC) versus the initial atrophy period (-1.52 FC), despite a similar
1280 average FC between recovery and control (0.1 FC). Mitochondrial fusion (*Mfn1/*2), transport (*Slc25a4)*
1281 and biogenesis (*Ppargc1a*) genes also significantly decreased after atrophy and/or repeated atrophy
1282 whereas *Tfam* significantly increased after repeated atrophy (**figure 8J**). Most genes recovered during
1283 TTX cessation, and *Opa1* and *Ppif* genes both significantly increased during recovery (**Figure 8J**). As
1284 with the ETC genes described above, there was a greater average reduction across all genes (excluding
1285 *Tfam* which increased) after repeated atrophy (-2.23 FC) compared to previous atrophy (-1.56 FC)
1286 relating to a 43% larger reduction after repeated atrophy compared to initial atrophy, where most genes
1287 recovered upon returning to activity (average 0.72 FC) (**Figure 8I & J**). At the protein level, there were
1288 no significant changes in protein abundance of ETC complexes I-V nor citrate synthase across the
1289 conditions analysed (e.g., sham, atrophy and recovery respectively, **Figure 8L)**. Finally, there was a
1290 reduction in mtDNA content during atrophy (-18%), recovery (-41%) and the greatest reduction after
1291 repeated atrophy (-50%) when *Mt-Rnr1* and *Mt-Rnr2* genes were combined (**Figure 8M).**
1292
1293
1294

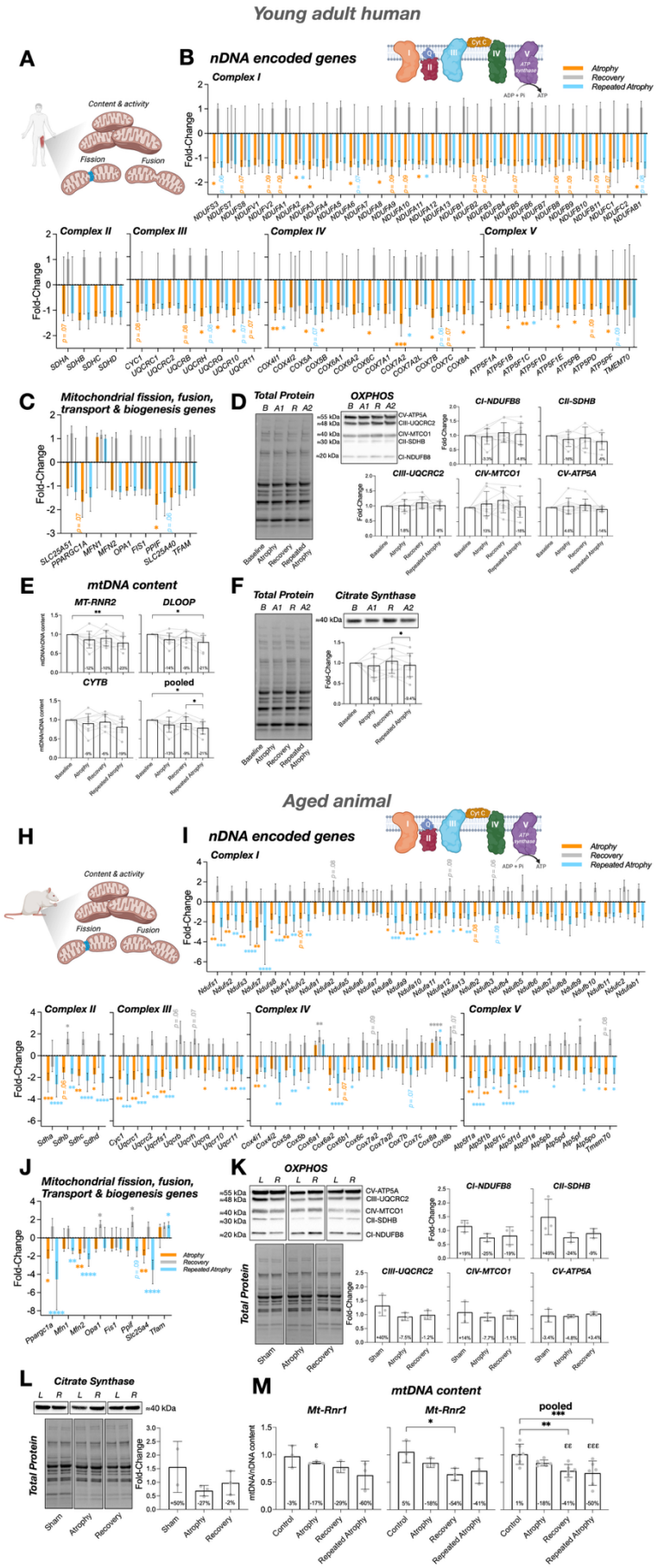
Young adult human
A
B nDNA encoded genes
Complex I
Atrophy
Recovery
Repeated Atrophy
Content & activity
Fission
Fusion
Fold-Change
Complex II
Complex III
Complex IV
Complex V
C Mitochondrial fission, fusion, transport & biogenesis genes
D Total Protein
OXPHOS
CI-NDUFB8
CII-SDHB
CIII-UQCRC2
CIV-MTCO1
CV-ATP5A
E mtDNA content
MT-RNR2
DLOOP
CYTB
pooled
F Total Protein
Citrate Synthase
Baseline
Atrophy
Recovery
Repeated Atrophy
Aged animal
H
I nDNA encoded genes
J Mitochondrial fission, fusion, Transport & biogenesis genes
K OXPHOS
Total Protein
Sham
L Citrate Synthase
M mtDNA content
Mt-Rnr1
Mt-Rnr2
pooled
Control

1295

Figure 8. Mitochondrial response to repeated periods of disuse in young adult human muscle (**A-G**) and aged rat muscle (**H-M**) skeletal muscle. (**A & H**) Schematic depicting a specific focus on mitochondrial content as well as mitochondrial activity, fusion and fission processes (created using BioRender.com). (**B & I**) Temporal transcriptional response of ETC complex I-V genes where most genes significantly decreased after atrophy and/or repeated atrophy, and recovered upon returning to normal activity in both adult humans (**B**) and aged animals (**I**). A similar transcriptional response occurred for mitochondrial fission, fusion, transport and biogenesis-related genes across species (**C & J**). There were no significant changes in ETC complex (I-V) protein abundance in both human (**D**) and rat (**K**) muscle. However, mtDNA content and citrate synthase protein significantly decreased after repeated atrophy in young adult humans (**E & F**). Despite no significant changes in citrate synthase across the sham/atrophy/repeated atrophy conditions analysed in aged animals (**L**), there was a reduction in mtDNA content in response to atrophy, recovery and repeated atrophy with the largest loss of -50% after repeated atrophy (**M**). Gene expression data presented as mean (signed) FC ± absolute 95% CI (absolute upper and lower limits). *$p \leq 0.05$, **$p \leq 0.01$, ***$p \leq 0.001$, ****$p \leq 0.0001$.

Discussion

Summary of main findings

Skeletal muscle exhibits a molecular memory of repeated disuse-induced atrophy. In young adult humans, repeated immobilization induced a comparable loss of skeletal muscle with full recovery between periods of disuse. Repeated disuse triggered a *protective* molecular resilience in which transcriptional perturbations of genes associated with oxidative metabolism and mitochondria (structure and function) were attenuated during recurrent atrophy. In contrast, aged muscle displayed a *detrimental* molecular susceptibility, characterised by further suppression of genes within similar pathways following repeated disuse, despite transcriptional recovery and continued muscle wasting upon returning to normal habitual activity. Proteasomal, ECM, and DNA damage associated genes were uniquely elevated following repeated atrophy in aged muscle. Methylome analyses revealed conserved epigenetic regulation of aerobic metabolism and mitochondrial genes across species, along with locus-specific memory genes including *NR4A1* and acetylcholine receptor subunit genes. Notably, nicotinamide riboside (NR) supplementation in human primary MuSC partially restored *NMRK1/2* expression and imrpoved myotube size in MuSC derived post-atrophy.

Molecular memory of repeated disuse-induced skeletal muscle atrophy

Skeletal muscle can retain an epigenetic 'memory' of prior growth, as demonstrated by persistent hypomethylation during detraining in humans and mice [33, 36, 37], and amplified gene expression upon retraining [33, 34, 36, 37]. Our findings now extend this concept to a clinically relevant negative stimulus. Specifically, disuse-induced atrophy which commonly occurs after injury, hospitalization, bed rest, surgery, or spaceflight. Crucially, we identified an age-dependent molecular memory: a *protective* transcriptional attenuation in young muscle, where repeated disuse elicited blunted transcriptional responses, and a *detrimental* memory in aged muscle, where repeated atrophy exaggerated suppression of NAD^+, aerobic metabolism and mitochondrial gene pathways.

Attenuated transcriptional memory in young adult humans and a detrimental exaggerated transcriptional memory in aged animal muscle

In young adult human muscle, genes suppressed during initial atrophy largely recovered and were less perturbed by repeated disuse, indicating a transcriptional protection or resilience. These responses

1337 predominantly involved oxidative metabolism and mitochondrial pathways, including TCA cycle,
1338 NAD^+/NADH, ETC, ATP synthesis. In contrast, aged animal muscle showed the opposite pattern, in
1339 which these same pathways were further suppressed during repeated atrophy despite transcriptional
1340 recovery after the initial disuse, accompanied by unique activation of proteasomal, ECM, and DNA
1341 damage gene pathways after repeated atrophy. These signatures are consistent ageing-associated
1342 skeletal muscle deficits in metabolic regulation, proteostasis, NMJ dysfunction (discussed below) and
1343 mitochondrial function [10, 19, 92]. Importantly, expression of these gene pathways recovered even though
1344 muscle mass continued to decline in aged muscle, confirming that the exaggerated transcriptional and
1345 physiological responses reflected a detrimental molecular memory rather than incomplete recovery of
1346 these molecular pathways.
1347
1348 *Mitochondrial vulnerability and loss of mtDNA with repeated disuse atrophy*

1349 Repeated disuse caused significant loss of mtDNA that was not evident after the initial atrophy period
1350 in either young adults or aged animals, with the most pronounced decline observed in aged muscle.
1351 These findings align previous bed rest studies demonstrating broad downregulation of mitochondria
1352 and reduced content/respiration during unloading [24, 64, 93]. Our transcriptomic data also revealed
1353 widespread suppression of electron transport chain and mitochondrial genes during atrophy and
1354 repeated atrophy, followed by recovery upon reloading/a return to activity. Although aged muscle
1355 exhibited the greatest mitochondrial vulnerability, young muscle also exhibited a marked loss of mtDNA
1356 loss after repeated atrophy, despite the transcriptional protection discussed above. This suggests that
1357 repeated disuse increases susceptibility to mitochondrial loss, raising the question as to whether further
1358 atrophic episodes of disuse atrophy could drive even young muscle toward the detrimental molecular
1359 program observed in aged muscle.

1360 *A similar epigenetic program in both species represses aerobic metabolism genes*

1361 Integrative methylome and transcriptome analyses revealed differentially methylated, differentially
1362 expressed genes (DmDEGs) enriched in oxidative metabolism and mitochondrial structure/turnover in
1363 both humans and rats. These genes were hypermethylated and downregulated during atrophy and
1364 repeated atrophy, returning toward baseline on recovery. This extends prior observations of disuse-
1365 linked methylation (e.g., nNOS hypermethylation [65], *Chrna1* hypomethylation/upregulation [66]) and
1366 contrasts with the hypomethylating effects of exercise training, higher physical activity and aerobic
1367 fitness associated with a 'younger' skeletal muscle methylome [36, 37, 39, 48, 57, 58, 59, 60, 63].

1368 *Neuromuscular signalling pathways in response to repeated atrophy: Epigenetic priming of the AChR*
1369 *subunit genes*

1370 Repeated disuse increased expression of acetylcholine receptor subunits, *CHRNA1, CHRND* in young
1371 human muscle, alongside hypomethylation at these loci, and similarly elevated *Chrna1, Chrnd, and*
1372 *Chrng* expression in aged rat muscle. Although potentially compensatory, such extra-junctional
1373 expression, especially of the fetal-type gamma subunit (*Chrng*), is typically linked to NMJ dysfunction

rather than stabilization [10]. In young muscle, this response emerged only after repeated atrophy, coinciding with the strongest hypomethylation, suggesting an epigenetic memory within AChR genes. Aged muscle demonstrated over a doubling in the upregulation of *Chrna1* (16-fold) and *Chrnd* (12.5-fold) after repeated disuse compared with initial disuse (*Chrna1* 7-fold, *Chrnd*-5.8 fold), and only significant elevation of *Chrng* after repeated atrophy. Whilst we did not detect hypomethylation of these genes in aged rat muscle, prior studies have also reported *Chrna1* hypomethylation in young adult rats utilised the same model of disuse [66]. Therefore, despite general transcriptional resilience, young muscle still exhibited exaggerated AChR gene responses to repeated atrophy. Further, the exaggerated response in aging muscle is consistent with aging studies associating poor recovery with NMJ instability and ER stress [10, 26, 94], and imply that repeated stress, even in young muscle, may epigenetically prime these genes, heightening vulnerability to future disuse.

NR supplementation partially restored NMRK2 levels and increased myotube size in human MuSC derived post-atrophy

NMRK2, a key NAD^+ salvage enzyme, was among most downregulated genes after both periods of atrophy in young adult humans and was significantly downregulated in aged rat muscle after repeated atrophy only, with broader NAD^+/NADH metabolism pathway repression across species, most pronounced in aged muscle. In primary human MuSC derived post-atrophy, nicotinamide riboside (NR) partially restored *NMRK2* and *MYOG* expression and improved myotube size, suggesting NAD^+ salvage as a potential target. However, whilst this provides initial *in-vitro* evidence, preclinical work shows intravenous NR elevates muscle NAD^+, while oral NR trials report mixed efficacy [91, 95]. Rigorous clinical studies in older, immobilization-prone populations are essential before considering NR as a viable therapeutic intervention.

ECM remodelling during recovery and repeated atrophy in aged muscle

Only aged muscle upregulated genes linked to extracellular matrix (ECM), collagen organization, collagen binding and sarcomere structure during recovery from initial disuse. This suggests structural remodelling as a compensatory response, which may stabilize tissue but also increase stiffness [96, 97], a hallmark of muscle aging, and therefore perhaps impair functional recovery. Further, ECM turnover, proteasomal pathways, and ubiquitin-mediated proteolysis were exclusively enriched after repeated atrophy in aged muscle, reinforcing the concept of compromised resilience to repeated disuse with age.

The NR4A genes are important metabolic regulators of repeated disuse atrophy in young human muscle

NR4A1, a key energy metabolism gene, was hypermethylated and remained downregulated even after full recovery in young muscle, while *NR4A3* showed the largest reduction of all altered genes (ranked 1st out of 384). Temporal profiling confirmed both genes retained suppression post-atrophy, indicating transcriptional memory. NR4A genes are highly responsive to exercise and inactivity [98]; *NR4A1* is oppositely hypomethylated and upregulated after high-intensity exercise [46], and *NR4A3* overexpression

1412 in rats enhances mitochondrial content, ATP production, and type-IIA & IIX muscle fibre protein content
1413 [99, 100, 101]. Knockdown of *NR4A3* impairs glucose metabolism and protein synthesis in skeletal muscle
1414 [102]. Collectively, these findings nominate *NR4A* genes as candidate targets to improve recovery and
1415 protect against future disuse atrophy.

1416 *Limitations*

1417 This study provides a comprehensive physiological and molecular analysis of repeated disuse atrophy
1418 across young adult human and aged rat skeletal muscle. However, several limitations should be
1419 acknowledged. 1) Interpretation of molecular protection vs. atrophy outcomes: While we observed
1420 transcriptional attenuation in young human muscle following repeated disuse, this did not translate into
1421 attenuated muscle mass loss. The term “protective molecular memory” refers specifically to reduced
1422 transcriptional responsiveness in metabolic pathways, not an attenuated loss in skeletal muscle size
1423 due to repeated atrophy. Further, whilst there was a predominance of molecular attenuation in young
1424 human muscle to repeated atrophy, there were also more susceptible losses, such as further mtDNA
1425 content and exaggerated increases in AChR subunit gene expression (discussed above). However, this
1426 raises the interesting question as to whether further atrophic episodes of disuse atrophy could drive
1427 even young muscle toward the detrimental program observed in aged muscle. 2) Coss-species
1428 comparisons and protocol differences: Although both models were analysed independently before
1429 integration, differences in species, disuse protocols (immobilization vs. TTX), recovery durations, and
1430 age must be considered when interpreting cross-species comparisons. Nonetheless, the conserved
1431 transcriptional and epigenetic responses across species, particularly in metabolic, mitochondrial and
1432 NAD^+ pathways, are notable and warrant further investigation. 3) Recovery protocol and activity
1433 monitoring: In aged rats, molecular pathways recovered during TTX cessation despite continued muscle
1434 wasting, suggesting that the transcriptional response was TTX-atrophy dependent rather than a
1435 consequence of incomplete recovery. Further, we present a comparison of the aged rats with young
1436 adult rats [66] that recover half of their muscle mass following a longer period of TTX-atrophy (and thus
1437 greater muscle wasting than aged animals herein) in a shorter recovery period. However, whilst rat
1438 activity was confirmed by the animals being able to perform dorsiflexion, activity levels during recovery
1439 was not directly measured. Future studies should incorporate behavioural tracking or respirometry in
1440 animals and make further control for nutrition and activity during human immobilization considering
1441 wearables (accelerometers) or bed-rest protocols to better characterize recovery dynamics and
1442 disentangle molecular recovery from functional outcomes. 4) Methodological constraints and data
1443 integration: The integration of multi-omics data across species and models introduces complexity. While
1444 individual analyses are robust, interpretation of age-related effects must consider differences. For
1445 example, due to limited fibre number in the cross-sections from human samples we also inferred fibre
1446 proportions using MYH and MYL gene expression data. Further, ETC protein data were not available
1447 for repeated atrophy in aged rats, and ETC protein changes were not statistically significant despite
1448 transcriptomic, NAD^+ content and mtDNA evidence of impairment. 5) Translational scope and *in vitro*
1449 validation: NR supplementation partially restored *NMRK2* expression and myotube size in post-atrophy
1450 human MuSCs, suggesting a potential therapeutic avenue. However, these findings are limited to *in*

vitro experiments in young adult cells. Further studies are needed to validate NAD^+ salvage interventions in aged muscle and *in vivo* models of repeated disuse. 6) Epigenetic interpretation and functional relevance: While DNA methylation changes were inversely associated with gene expression in key metabolic pathways, functional consequences of these epigenetic modifications remain to be fully elucidated. Future work should explore whether these methylation signatures directly modulate transcriptional memory or serve as biomarkers of prior disuse.

Future mechanistic and clinical directions

We propose mechanistic and translational studies that address testable hypothesis, such as: (i) Does enhancing NAD^+ salvage attenuate the maladaptive transcriptional response to repeated disuse in aged muscle? ii) Does exercise 'preconditioning' [103, 104] or training reprogram methylation signatures to prevent negative molecular memory in the nuclear [39, 57] and mitochondrial genome [63]? (iii) does targeted activation of *NR4A* family and *NMRK2* genes during atrophy or recovery prevent or offset disuse-induced atrophy and/or promote recovery from atrophy?

Conclusion

Disuse atrophy can be remembered at the molecular level in skeletal muscle. It is predominantly protective in young skeletal muscle yet detrimental in aged skeletal muscle. This memory is partially epigenetically encoded at the single locus level and converges in aerobic metabolism, mitochondrial and NAD^+ pathways, and nominates molecular targets to preserve muscle mass and function after recurrent immobilization or disuse.

Acknowledgements

This research was funded by the Research Council of Norway (RCN) (314157) awarded to principal investigator Adam P. Sharples, post-doc fellow Daniel C. Turner and co-investigators Sue Bodine, Jonathan C. Jarvis, David C. Hughes, Daniel J. Owens, Truls Raastad and Olivier Seynnes. We thank Olivier Seynnes for his critical expertise and input into the funding application, training & supervision of post-doctoral researcher for the design, testing and analysis of the human experiments and associated physiological data acquisition and analysis (muscle size/CSA & strength). We thank Jostein Hallèn, Siri T. Dalen, Hege N. Ødemark and Emil Løvstakken (NIH) for assistance with muscle biopsies and tissue processing; Josephine A. Eyrich (UCPH) for assisting with the measurements of NAD^+ content; Rune Enger, as the medical lead for the human biopsies; Enovis/DJO LLC for kindly donating the knee braces and to; ChromaDex Inc. for providing nicotinamide riboside for *in vitro* studies. Finally, sincere gratitude to all participants who volunteered to participate in this study that included two periods of muscle wasting.

Author contributions

Adam P. Sharples conceived the project, secured funding as principal investigator, and led the human experimental design, ethical approvals, data/finance management, dissemination, and oversaw analysis of all human and rat experiments, and supervised postdoctoral fellow Daniel C. Turner. Daniel C. Turner conducted most of the experimental work, including recruitment, human testing, biopsy processing, wet lab work, data collection, analysis, visualization, dissemination and manuscript drafting. Jonathan C. Jarvis supervised and undertook the animal intervention studies with Hazel Sutherland and provided vital input into the funding application and expertise in experimental design, analysis and interpretation. Sue C. Bodine, David C. Hughes, Daniel J Owens, and Truls Raastad were co-investigators in the funding application and heavily involved in study design, biopsy sampling, interpretation of results, and manuscript preparation. Stian F. Christiansen undertook experimental work for the mtDNA analysis in MuSC. Jonas T. Treebak and Emilie D. Kellezi undertook NAD^+ content experiments. Eva Wozniak, Charles Mein and James Boot undertook RNA-seq and RRBS/RREM wet lab experiments and pre-processing of RNA-seq, RRBS/RREM and bioinformatics. Max Ullrich assisted in omics analysis and visualization. All authors contributed significantly to the final manuscript.

Declarations and conflicts

The authors declare no conflicting interests. ChromaDex provided the nicotinamide riboside for *in-vitro* experiments but had no influence on the study.

Data availability

RNA-seq and RRBS/RREM data will be available via the Gene Expression Omnibus (GEO) repository (or equivalent once accepted for publication. Any other source of processed data is available on reasonable request to the corresponding authors.

Software and Code availability

All analysis code used for preprocessing, normalization, differential expression/methylation, enrichment and visualization of the data is freely available and references and links have been provided in the methods. All code that is not freely available is available on reasonable request to the corresponding authors.

References

1. Hughes VA, *et al.* Longitudinal muscle strength changes in older adults: influence of muscle mass, physical activity, and health. *J Gerontol A Biol Sci Med Sci* **56**, B209-217 (2001).

2. Cruz-Jentoft AJ, Landi F, Topinkova E, Michel JP. Understanding sarcopenia as a geriatric syndrome. *Current opinion in clinical nutrition and metabolic care* **13**, 1-7 (2010).

3. Beaudart C, Zaaria M, Pasleau F, Reginster J-Y, Bruyère O. Health Outcomes of Sarcopenia: A Systematic Review and Meta-Analysis. *PLOS ONE* **12**, e0169548 (2017).

4. Fried LP, *et al.* Frailty in Older Adults: Evidence for a Phenotype. *The Journals of Gerontology: Series A* **56**, M146-M157 (2001).

5. Rejc E, *et al.* Loss of maximal explosive power of lower limbs after 2 weeks of disuse and incomplete recovery after retraining in older adults. *J Physiol* **596**, 647-665 (2018).

6. Pisot R, *et al.* Greater loss in muscle mass and function but smaller metabolic alterations in older compared with younger men following 2 wk of bed rest and recovery. *J Appl Physiol (1985)* **120**, 922-929 (2016).

7. Kramer IF, *et al.* Extensive Type II Muscle Fiber Atrophy in Elderly Female Hip Fracture Patients. *J Gerontol A Biol Sci Med Sci* **72**, 1369-1375 (2017).

8. Suetta C, *et al.* Effects of aging on human skeletal muscle after immobilization and retraining. *J Appl Physiol (1985)* **107**, 1172-1180 (2009).

9. Baehr LM, West DWD, Marshall AG, Marcotte GR, Baar K, Bodine SC. Muscle-specific and age-related changes in protein synthesis and protein degradation in response to hindlimb unloading in rats. *J Appl Physiol (1985)* **122**, 1336-1350 (2017).

10. Baehr LM, *et al.* Age-related deficits in skeletal muscle recovery following disuse are associated with neuromuscular junction instability and ER stress, not impaired protein synthesis. *Aging (Albany NY)* **8**, 127-146 (2016).

11. Hvid L, *et al.* Effects of aging on muscle mechanical function and muscle fiber morphology during short-term immobilization and subsequent retraining. *J Appl Physiol (1985)* **109**, 1628-1634 (2010).

12. Reidy PT, *et al.* Aging impairs mouse skeletal muscle macrophage polarization and muscle-specific abundance during recovery from disuse. *Am J Physiol Endocrinol Metab* **317**, E85-e98 (2019).

13. Bodine SC, *et al.* Identification of ubiquitin ligases required for skeletal muscle atrophy. *Science* **294**, 1704-1708 (2001).

14. Dirks ML, Wall BT, Snijders T, Ottenbros CL, Verdijk LB, van Loon LJ. Neuromuscular electrical stimulation prevents muscle disuse atrophy during leg immobilization in humans. *Acta Physiol (Oxf)* **210**, 628-641 (2014).

15. Kilroe SP, Fulford J, Jackman SR, LJC VANL, Wall BT. Temporal Muscle-specific Disuse Atrophy during One Week of Leg Immobilization. *Med Sci Sports Exerc* **52**, 944-954 (2020).

16. Jameson TSO, *et al.* Muscle damaging eccentric exercise attenuates disuse-induced declines in daily myofibrillar protein synthesis and transiently prevents muscle atrophy in healthy men. *Am J Physiol Endocrinol Metab* **321**, E674-e688 (2021).

17. Wall BT, Dirks ML, Snijders T, Senden JMG, Dolmans J, van Loon LJC. Substantial skeletal muscle loss occurs during only 5 days of disuse. *Acta Physiologica* **210**, 600-611 (2014).

18. Wall BT, *et al.* Short-term muscle disuse lowers myofibrillar protein synthesis rates and induces anabolic resistance to protein ingestion. *Am J Physiol Endocrinol Metab* **310**, E137-147 (2016).

19. Franchi MV, *et al.* Previous short-term disuse dictates muscle gene expression and physiological adaptations to subsequent resistance exercise. *J Physiol* **603**, 3725-3753 (2025).

20. Brocca L, *et al.* Human skeletal muscle fibre contractile properties and proteomic profile: adaptations to 3 weeks of unilateral lower limb suspension and active recovery. *J Physiol* **593**, 5361-5385 (2015).

21. Campbell EL, *et al.* Skeletal muscle adaptations to physical inactivity and subsequent retraining in young men. *Biogerontology* **14**, 247-259 (2013).

22. Dirks ML, *et al.* One Week of Bed Rest Leads to Substantial Muscle Atrophy and Induces Whole-Body Insulin Resistance in the Absence of Skeletal Muscle Lipid Accumulation. *Diabetes* **65**, 2862-2875 (2016).

23. Bamman MM, *et al.* Impact of resistance exercise during bed rest on skeletal muscle sarcopenia and myosin isoform distribution. *J Appl Physiol (1985)* **84**, 157-163 (1998).

24. Noone J, *et al.* The impact of 60 days of -6° head down tilt bed rest on mitochondrial content, respiration and regulators of mitochondrial dynamics. *J Physiol* **603**, 3777-3794 (2025).

25. Ringholm S, *et al.* Bed rest reduces metabolic protein content and abolishes exercise-induced mRNA responses in human skeletal muscle. *Am J Physiol Endocrinol Metab* **301**, E649-658 (2011).

26. Motanova E, *et al.* Neuromuscular junction instability with inactivity: morphological and functional changes after 10 days of bed rest in older adults. *J Physiol*, (2025).

27. Edgerton VR, *et al.* Human fiber size and enzymatic properties after 5 and 11 days of spaceflight. *J Appl Physiol (1985)* **78**, 1733-1739 (1995).

28. Murgia M, *et al.* Spaceflight on the ISS changed the skeletal muscle proteome of two astronauts. *NPJ Microgravity* **10**, 60 (2024).

29. Murgia M, *et al.* Signatures of muscle disuse in spaceflight and bed rest revealed by single muscle fiber proteomics. *PNAS Nexus* **1**, pgac086 (2022).

30. Sharples AP, Stewart CE, Seaborne RA. Does skeletal muscle have an 'epi'-memory? The role of epigenetics in nutritional programming, metabolic disease, aging and exercise. *Aging cell* **15**, 603-616 (2016).

31. Sharples AP, Turner DC. Skeletal muscle memory. *Am J Physiol Cell Physiol* **324**, C1274-c1294 (2023).

32. Bruusgaard JC, Johansen IB, Egner IM, Rana ZA, Gundersen K. Myonuclei acquired by overload exercise precede hypertrophy and are not lost on detraining. *Proc Natl Acad Sci U S A* **107**, 15111-15116 (2010).

33. Wen Y, Dungan CM, Mobley CB, Valentino T, von Walden F, Murach KA. Nucleus Type-Specific DNA Methylomics Reveals Epigenetic "Memory" of Prior Adaptation in Skeletal Muscle. *Function (Oxf)* **2**, zqab038 (2021).

34. Weidenhamer CJ, Huang YH, Natua S, Kalsotra A, Hernández-Saavedra D. Muscle memory of exercise optimizes mitochondrial metabolism to support skeletal muscle growth. *Am J Physiol Cell Physiol* **329**, C1239-c1255 (2025).

35. Egner IM, Bruusgaard JC, Eftestøl E, Gundersen K. A cellular memory mechanism aids overload hypertrophy in muscle long after an episodic exposure to anabolic steroids. *J Physiol* **591**, 6221-6230 (2013).

36. Seaborne RA*, et al.* Human Skeletal Muscle Possesses an Epigenetic Memory of Hypertrophy. *Scientific Reports (Nature)* **8**, 1898 (2018).

37. Turner DC, Seaborne RA, Sharples AP. Comparative Transcriptome and Methylome Analysis in Human Skeletal Muscle Anabolism, Hypertrophy and Epigenetic Memory. *Scientific reports* **9**, 4251 (2019).

38. Hulmi JJ*, et al.* Human skeletal muscle possesses both reversible proteomic signatures and a retained proteomic memory after repeated resistance training. *J Physiol*, (2025).

39. Blocquiaux S*, et al.* Recurrent training rejuvenates and enhances transcriptome and methylome responses in young and older human muscle. *JCSM Rapid Communications* **5**, 10-32 (2022).

40. Pilotto AM*, et al.* Human skeletal muscle possesses an epigenetic memory of high-intensity interval training. *Am J Physiol Cell Physiol* **328**, C258-c272 (2025).

41. Sexton CL*, et al.* Skeletal Muscle DNA Methylation and mRNA Responses to a Bout of Higher versus Lower Load Resistance Exercise in Previously Trained Men. *Cells* **12**, (2023).

42. Rowlands DS*, et al.* Multi-omic integrated networks connect DNA methylation and miRNA with skeletal muscle plasticity to chronic exercise in Type 2 diabetic obesity. *Physiological Genomics* **46**, 747-765 (2014).

43. Edman S*, et al.* The 24-hour molecular landscape after exercise in humans reveals MYC is sufficient for muscle growth. *EMBO reports* **25**, 5810-5837 (2024).

44. Von Walden F*, et al.* The myonuclear DNA methylome in response to an acute hypertrophic stimulus. *Epigenetics* **15**, 1151-1162 (2020).

45. Chambers TL*, et al.* Methylome–proteome integration after late-life voluntary exercise training reveals regulation and target information for improved skeletal muscle health. *The Journal of Physiology* **603**, 211-237 (2025).

46. Maasar MF*, et al.* The Comparative Methylome and Transcriptome After Change of Direction Compared to Straight Line Running Exercise in Human Skeletal Muscle. *Front Physiol* **12**, 619447 (2021).

47. Jacques M*, et al.* Methylome and proteome integration in human skeletal muscle uncover group and individual responses to high-intensity interval training. *Faseb j* **37**, e23184 (2023).

48. Gorski PP*, et al.* Aerobic exercise training resets the human skeletal muscle methylome 10 years after breast cancer treatment and survival. *Faseb j* **37**, e22720 (2023).

49. Gorski PP, Turner DC, Iraki J, Morton JP, Sharples AP, Areta JL. Human skeletal muscle methylome after low-carbohydrate energy-balanced exercise. *American Journal of Physiology-Endocrinology and Metabolism* **324**, E437-E448 (2023).

50. Barrès R*, et al.* Acute exercise remodels promoter methylation in human skeletal muscle. *Cell Metab* **15**, 405-411 (2012).

51. Nitert MD*, et al.* Impact of an Exercise Intervention on DNA Methylation in Skeletal Muscle From First-Degree Relatives of Patients With Type 2 Diabetes. *Diabetes* **61**, 3322-3332 (2012).

52. Geiger C*, et al.* DNA methylation of exercise-responsive genes differs between trained and untrained men. *BMC Biology* **22**, 147 (2024).

53. Furrer R*, et al.* Molecular control of endurance training adaptation in male mouse skeletal muscle. *Nature Metabolism* **5**, 2020-2035 (2023).

54. Lindholm ME*, et al.* An integrative analysis reveals coordinated reprogramming of the epigenome and the transcriptome in human skeletal muscle after training. *Epigenetics* **9**, 1557-1569 (2014).

55. Jacques M*, et al.* Molecular landscape of sex- and modality-specific exercise adaptation in human skeletal muscle through large-scale multi-omics integration. *Cell Rep* **44**, 115750 (2025).

56. Egan B, Sharples AP. Molecular responses to acute exercise and their relevance for adaptations in skeletal muscle to exercise training. *Physiol Rev* **103**, 2057-2170 (2023).

57. Voisin S*, et al.* Exercise is associated with younger methylome and transcriptome profiles in human skeletal muscle. *Aging cell*, e13859 (2023).

58. Sailani MR*, et al.* Lifelong physical activity is associated with promoter hypomethylation of genes involved in metabolism, myogenesis, contractile properties and oxidative stress resistance in aged human skeletal muscle. *Sci Rep* **9**, 3272 (2019).

59. Turner DC*, et al.* DNA methylation across the genome in aged human skeletal muscle tissue and muscle-derived cells: The role of HOX genes and physical activity. *Scientific reports* **10**, 15360 (2020).

60. Voisin S*, et al.* Meta-analysis of genome-wide DNA methylation and integrative omics of age in human skeletal muscle. *J Cachexia Sarcopenia Muscle* **12**, 1064-1078 (2021).

61. Zykovich A*, et al.* Genome-wide DNA methylation changes with age in disease-free human skeletal muscle. *Aging cell* **13**, 360-366 (2014).

62. Barrès R*, et al.* Non-CpG methylation of the PGC-1alpha promoter through DNMT3B controls mitochondrial density. *Cell Metab* **10**, 189-198 (2009).

63. Ruple BA*, et al.* Resistance training rejuvenates the mitochondrial methylome in aged human skeletal muscle. *Faseb j* **35**, e21864 (2021).

64. Alibegovic AC*, et al.* Insulin resistance induced by physical inactivity is associated with multiple transcriptional changes in skeletal muscle in young men. *American Journal of Physiology-Endocrinology and Metabolism* **299**, E752-E763 (2010).

65. Tomiga Y*, et al.* One week, but not 12 hours, of cast immobilization alters promotor DNA methylation patterns in the nNOS gene in mouse skeletal muscle. *The Journal of Physiology* **597**, 5145-5159 (2019).

66. Fisher AG*, et al.* Transcriptomic and epigenetic regulation of disuse atrophy and the return to activity in skeletal muscle. *Faseb j* **31**, 5268-5282 (2017).

67. Falick Michaeli T*, et al.* Muscle injury causes long-term changes in stem-cell DNA methylation. *Proc Natl Acad Sci U S A* **119**, e2212306119 (2022).

68. Lee PH, Macfarlane DJ, Lam TH, Stewart SM. Validity of the International Physical Activity Questionnaire Short Form (IPAQ-SF): a systematic review. *Int J Behav Nutr Phys Act* **8**, 115 (2011).

69. Li Y*, et al.* Active Ankle Movements Prevent Formation of Lower-Extremity Deep Venous Thrombosis After Orthopedic Surgery. *Med Sci Monit* **22**, 3169-3176 (2016).

70. Sarto F, *et al.* Effects of short-term unloading and active recovery on human motor unit properties, neuromuscular junction transmission and transcriptomic profile. *J Physiol* **600**, 4731-4751 (2022).

71. Skattebo Ø, Peci D, Clauss M, Johansen EI, Jensen J. Increased Mass-Specific Maximal Fat Oxidation Rate with Small versus Large Muscle Mass Exercise. *Med Sci Sports Exerc* **54**, 974-983 (2022).

72. Seaborne RA, *et al.* UBR5 is a novel E3 ubiquitin ligase involved in skeletal muscle hypertrophy and recovery from atrophy. *J Physiol* **597**, 3727-3749 (2019).

73. Elhassan YS, *et al.* OR03-06 NAD+ Availability Modulates 11β-HSD1-Mediated Glucocorticoid Regeneration in Mouse Skeletal Muscle. *J Endocr Soc* **4**, (2020).

74. Alsharidah M, Lazarus NR, George TE, Agley CC, Velloso CP, Harridge SD. Primary human muscle precursor cells obtained from young and old donors produce similar proliferative, differentiation and senescent profiles in culture. *Aging cell* **12**, 333-344 (2013).

75. Schmittgen TD, Livak KJ. Analyzing real-time PCR data by the comparative C(T) method. *Nat Protoc* **3**, 1101-1108 (2008).

76. Dobin A, *et al.* STAR: ultrafast universal RNA-seq aligner. *Bioinformatics* **29**, 15-21 (2013).

77. Love MI, Huber W, Anders S. Moderated estimation of fold change and dispersion for RNA-seq data with DESeq2. *Genome Biol* **15**, 550 (2014).

78. Tang D, *et al.* SRplot: A free online platform for data visualization and graphing. *PLoS One* **18**, e0294236 (2023).

79. Hulsen T. DeepVenn - a web application for the creation of area-proportional Venn diagrams using the deep learning framework Tensorflow.js. *ArXiv* **abs/2210.04597**, (2022).

80. Huang DW, Sherman BT, Lempicki RA. Systematic and integrative analysis of large gene lists using DAVID bioinformatics resources. *Nature Protocols* **4**, 44-57 (2009).

81. Smith T, Heger A, Sudbery I. UMI-tools: modeling sequencing errors in Unique Molecular Identifiers to improve quantification accuracy. *Genome Res* **27**, 491-499 (2017).

82. Krueger F, Andrews SR. Bismark: a flexible aligner and methylation caller for Bisulfite-Seq applications. *Bioinformatics* **27**, 1571-1572 (2011).

83. Akalin A, *et al.* methylKit: a comprehensive R package for the analysis of genome-wide DNA methylation profiles. *Genome Biol* **13**, R87 (2012).

84. Rooney JP, *et al.* PCR based determination of mitochondrial DNA copy number in multiple species. *Methods Mol Biol* **1241**, 23-38 (2015).

85. Lapatto HAK, *et al.* Nicotinamide riboside improves muscle mitochondrial biogenesis, satellite cell differentiation, and gut microbiota in a twin study. *Sci Adv* **9**, eadd5163 (2023).

86. Kemper MF, Stirone C, Krause DN, Duckles SP, Procaccio V. Genomic and non-genomic regulation of PGC1 isoforms by estrogen to increase cerebral vascular mitochondrial biogenesis and reactive oxygen species protection. *Eur J Pharmacol* **723**, 322-329 (2014).

87. Arduini A, *et al.* Mitochondrial biogenesis fails in secondary biliary cirrhosis in rats leading to mitochondrial DNA depletion and deletions. *Am J Physiol Gastrointest Liver Physiol* **301**, G119-127 (2011).

88. Stevanović-Silva J, Beleza J, Coxito P, Oliveira PJ, Ascensão A, Magalhães J. Gestational Exercise Antagonises the Impact of Maternal High-Fat High-Sucrose Diet on Liver Mitochondrial Alterations and Quality Control Signalling in Male Offspring. *Int J Environ Res Public Health* **20**, (2023).

89. Dall M*, et al.* Hepatic NAD+ levels and NAMPT abundance are unaffected during prolonged high-fat diet consumption in C57BL/6JBomTac mice. *Molecular and Cellular Endocrinology* **473**, 245-256 (2018).

90. Van der Stede T*, et al.* Deconvoluting fiber type proportions from human skeletal muscle transcriptomics and proteomics data using FibeRtypeR. *bioRxiv*, 2025.2009.2017.676778 (2025).

91. Damgaard MV, Treebak JT. What is really known about the effects of nicotinamide riboside supplementation in humans. *Sci Adv* **9**, eadi4862 (2023).

92. Bodine SC, Sinha I, Sweeney HL. Mechanisms of Skeletal Muscle Atrophy and Molecular Circuitry of Stem Cell Fate in Skeletal Muscle Regeneration and Aging. *The Journals of Gerontology: Series A* **78**, 14-18 (2023).

93. Zuccarelli L*, et al.* Mitochondrial Sensitivity to Submaximal [ADP] Following Bed Rest: A Novel Two-Phase Approach Associated With Fibre Types. *J Cachexia Sarcopenia Muscle* **16**, e13775 (2025).

94. Sarto F*, et al.* Twenty-one days of bed rest alter motor unit properties and neuromuscular junction transmission in young adults. *J Appl Physiol (1985)* **138**, 1411-1424 (2025).

95. Damgaard MV*, et al.* Intravenous nicotinamide riboside elevates mouse skeletal muscle NAD(+) without impacting respiratory capacity or insulin sensitivity. *iScience* **25**, 103863 (2022).

96. Stearns-Reider KM*, et al.* Aging of the skeletal muscle extracellular matrix drives a stem cell fibrogenic conversion. *Aging cell* **16**, 518-528 (2017).

97. Pavan P*, et al.* Alterations of Extracellular Matrix Mechanical Properties Contribute to Age-Related Functional Impairment of Human Skeletal Muscles. *International Journal of Molecular Sciences* **21**, 3992 (2020).

98. Pillon NJ*, et al.* Transcriptomic profiling of skeletal muscle adaptations to exercise and inactivity. *Nature Communications* **11**, 470 (2020).

99. White JR, Confides AL, Moore-Reed S, Hoch JM, Dupont-Versteegden EE. Regrowth after skeletal muscle atrophy is impaired in aged rats, despite similar responses in signaling pathways. *Exp Gerontol* **64**, 17-32 (2015).

100. Pearen MA*, et al.* The nuclear receptor, Nor-1, markedly increases type II oxidative muscle fibers and resistance to fatigue. *Mol Endocrinol* **26**, 372-384 (2012).

101. Goode JM*, et al.* The Nuclear Receptor, Nor-1, Induces the Physiological Responses Associated With Exercise. *Mol Endocrinol* **30**, 660-676 (2016).

102. Smith JAB*, et al.* Inactivity-induced NR4A3 downregulation in human skeletal muscle affects glucose metabolism and translation: Insights from in vitro analysis. *Mol Metab* **99**, 102200 (2025).

103. Brocca L, Rossi M, Canepari M, Bottinelli R, Pellegrino MA. Exercise Preconditioning Blunts Early Atrogenes Expression and Atrophy in Gastrocnemius Muscle of Hindlimb Unloaded Mice. *International Journal of Molecular Sciences* **23**, 148 (2022).

104. Michel JM, *et al.* Effects of leg immobilization and recovery resistance training on skeletal muscle-molecular markers in previously resistance-trained versus untrained adults. *Journal of Applied Physiology* **138**, 450-467 (2025).